LAWRENCE
LIVERMORE
NATIONAL
LABORATORY

LLNL-TR-843491

LSECE Data Release Report

R. L. Rodd

December 23, 2022

Disclaimer

This document was prepared as an account of work sponsored by an agency of the United States government. Neither the United States government nor Lawrence Livermore National Security, LLC, nor any of their employees makes any warranty, expressed or implied, or assumes any legal liability or responsibility for the accuracy, completeness, or usefulness of any information, apparatus, product, or process disclosed, or represents that its use would not infringe privately owned rights. Reference herein to any specific commercial product, process, or service by trade name, trademark, manufacturer, or otherwise does not necessarily constitute or imply its endorsement, recommendation, or favoring by the United States government or Lawrence Livermore National Security, LLC. The views and opinions of authors expressed herein do not necessarily state or reflect those of the United States government or Lawrence Livermore National Security, LLC, and shall not be used for advertising or product endorsement purposes.

This work performed under the auspices of the U.S. Department of Energy by Lawrence Livermore National Laboratory under Contract DE-AC52-07NA27344.

Date Release Report for Large Surface Explosion Coupling Experiment (LSECE)
Nevada National Security Site

December 2022

Compiled by:
Rebecca Rodd
Lawrence Livermore National Laboratory

With Contributions From:

Lawrence Livermore National Laboratory
William R. Walter, Sean Ford, Ethan Alger, Beth Dzenitis

Los Alamos National Laboratory
Phil Blom

Sandia National Laboratory
Robert Abbott, Daniel Bowman

Mission Support and Test Services, LLC
Cleat Zeiler, Robert White, Reagan Turley

NNSS Weather Operations, Air Resources Laboratory/Special Operations & Research Division
Walter Schalk

Nevada Seismological Laboratory, University of Nevada, Reno
Emily Morton, Gabe Plank

Disclaimer Page

Execution Team

Lawrence Livermore National Laboratory
Beth Dzenitis, Ethan Alger

Los Alamos National Laboratory
Ken Laintz

Sandia National Laboratory
Daniel Bowman , Robert Abbott, Zach Cashion

Defense Threat Reduction Agency
Ben Heshmatpour, David Williams, Richard Lewis

Mission Support and Test Services, LLC
Bob White, Cleat Zeiler, Douglas Seastrand, Ian McKenna, Gary Skougard, Lisa Garner

NNSS Weather Operations, Air Resources Laboratory/Special Operations & Research Division
Walter Schalk

Applied Research Associates

Desert Research Institute
George Nikolich

Other Major Contributors

Lawrence Livermore National Laboratory

Los Alamos National Laboratory

Sandia National Laboratory

Defense Threat Reduction Agency

Mission Support and Test Services, LLC

Applied Research Associates

Nevada Seismological Laboratory, University of Nevada, Reno

NNSS Weather Operations, Air Resources Laboratory/Special Operations & Research Division

Executive Summary

The DTRA sponsored 2020-2022 Large Surface Explosion Coupling Experiment (LSECE) consists of two large ground surface chemical explosions, data collection, analysis and modeling carried out in 2020-2022. The LSECE chemical explosions were carried out at the site of prior NNSA sponsored buried chemical explosions that were part of the Source Physics Experiment (SPE) Phase II in Dry Alluvium Geology (DAG). This report described the data collected under LSECE that is being made publicly available. The prior buried explosion DAG data are described in a separate report (https://www.osti.gov/biblio/1825534) and are also publicly available.

The LSECE explosions, data analysis and numerical modeling work sponsored by DTRA were intended to address three objectives:

1) Generate seismo-acoustic data to test and improve numerical models of explosion energy coupling in dry alluvium geology.
2) To improve seismo-acoustic yield estimation techniques as a function of depth and medium properties.
3) To study and improve acoustic propagation modeling under two different atmospheric conditions.

The LSECE data that were collected have expanded the prior DAG buried explosion dataset to include surface chemical explosions recorded on a common set of seismo-acoustic stations. They have allowed a more detailed study of above and below surface seismo-acoustic energy coupling with applications to explosion monitoring and assessment. The two approximately 1-ton TNT equivalent yield LSECE explosions were detonated at different times of the day to explore the effects of the different atmospheric conditions. The first chemical explosion "Artemis" was conducted before dawn when temperature inversions were present. The second chemical explosion "Apollo" was conducted on a sunny afternoon when the temperature gradient was more linear.

The LSECE chemical explosion data were also collected across a variety of different sensor types to allow evaluation of their effectiveness in recovering useful information. The LSECE instrumentation included fiber optic or Distributed Acoustic Sensing (DAS), a dense array or Large-N array of seismometers, borehole accelerometers, DAS and a velocity meter, airborne acoustic instruments and a variety of visual and remote sensing data.

Much initial analysis and modeling has been done with the LSCE data by the team members. This work has been presented at professional Society conferences and written up in peer-reviewed papers in various stages of completion. These include: Blom (2022); Chen et al

(2022); Euser and Delorey (2022); Garces et al. (2022); Pyle and Walter (2021); Vorobiev (2022) and Waxler et al (2022).

The public release of the LSECE data accompanying this report will allow peer review of the work done so far as well as stimulate new analysis and discovery in the years ahead. The authors of this data report would appreciate hearing about further analysis using this data along with any questions or issues that come up. Finally, the authors of this report thank the hard work by the execution teams that successfully carried out LSECE during the time of a global pandemic with excellent results and data return.

References:

Blom., P. (2022) "Regional infrasonic observations from surface explosions – influence of atmospheric variations." *Geophysical Journal International.* In Preparation

Chen, T., Larmat, C., & Blom, P. (2022) "Seismoacoustic analysis of surface explosions using a Large-N seismic array." *Bulletin of the Seismological Society of America.* In Preparation.

Euser, B. & Delorey, A. (2022) "Modeling of a surface explosion using HOSS Fluid-Surface interface Solver (FSIS)". LANL Report. In preparation.

Garcés, M.A.; Bowman, D.; Zeiler, C.; Christe, A.; Yoshiyama, T.; Williams, B.; Colet, M.; Takazawa, S.; Popenhagen, S. Skyfall: Signal Fusion from a Smartphone Falling from the Stratosphere. *Signals* **2022**, *3*, 209–234. https://doi.org/10.3390/signals3020014

Pyle, M. L., and W. R. Walter (2021). Exploring the Effects of Emplacement Conditions on Explosion P/S Ratios Across Local to Regional Distances, Seismol. Res. Lett., 93, 866–879, doi: 10.1785/0220210270.

Waxler, R., Hetzer, C., Assink, J., & Blom, P. (2022) "A 2D effective sound speed parabolic equation with ground topography." *Journal of the Acoustical Society of America.* In DTRA Review.

Vorobiev, O. (2022) Near field modeling of the Large Explosion Coupling Experiment. In Preparation.

Table of Contents

List of Attachments

List of Figures

List of Tables

1 Introduction

The Large Surface Explosion Coupling Experiment (LSECE) is a DTRA sponsored project consisting of two surface explosions with extensive data collection, followed by two years of data analysis and modeling. LSECE was designed to take advantage of the prior NNSA sponsored Source Physics Experiment (SPE) Phase II Dry Alluvium Geology (DAG) - buried explosions and the sensor network that recorded them – to allow comparisons between surface and buried explosions and exploration of seismoacoustic coupling and propagation issues.

2 Test Objectives

The two LSECE surface explosions were conducted above the four buried DAG explosions to allow comparisons between the different emplacement conditions on the signatures the explosions produced. The two surface explosions were conducted at different times in order to have different atmospheric conditions. The first show Artemis was conducted before dawn when the atmospheric temperature profile had several small inversions. Apollo, the second shot was conducted on a sunny afternoon when the atmospheric temperature profile showed no inversions.

3 Site Description

The LSECE chemical explosions were carried out on the ground surface above the four buried DAG explosions. The DAG test bed consists of a cleared pad in an open and flat area of northern Yucca Flat. There is minimal fill across the pad surface and the substrate is alluvium. The water table depth was below any of the buried DAG explosions, the deepest of which was at about 385m below the surface. More details about the DAG site can be found in the DAG data release report.

4 Test Descriptions

LSECE consists of two surface detonations of 1800 lbs commercial-grade C-4 with 8 RP-83 detonators about 100 feet from the Dry Alluvium Geology (DAG) Ground Zero (GZ). Shot details are in Table 1.

Name	**Date & Time (UTC)**	**Location (Latitude, Longitude)**	**Package dimensions (LxWxH inch)**	**Package weight (lbs HE type)**	**TNT-equivalent* (kg)**
Artemis	2020/10/27 (301) 13:37:10.63790412	37.114912493, -116.069089728	45-1/2x37x29-1/4	1807.6 C-4	992.1
Apollo	2020/10/29 (303) 22:35:34.31303666	37.114912493, -116.069089728	46x37x29-1/4	1806.5 C-4	991.5

Table 1: LSECE shot locations and summary descriptions.

4.1 Artemis

Artemis was detonated at 13:37:10.63790412 UTC (6:37 AM local PDT) on Tuesday, October 27, 2020 (Julian Date 301 2020). The yield was 0.99205 metric tons (992.05 kg) TNT-equivalent chemical explosion (based on 819.9 kg of C-4 and using a 1.21 TNT equivalency factor).

Explosives dimensions were: 45.5” (L) x 37” (W) x 29.25” (H) (1.1557 m x 0.9398 m x 0.74295 m). Explosive height was 6.5 inches above the ground (on a plastic pallet). The location was 37.114912493 N and. -116.069089728 W, approximately 33. 2 m ENE of DAG explosions GZ. The local seismic magnitude according to University of Nevada, Reno (UNR) catalog is ML about 0.43.

4.2 Apollo

Apollo was detonated in an approximately 1 m deep by 3-4 m wide crater created by Artemis at 22:35:34.31303666 UTC (3:35 PM local PDT) on Thursday, October 29, 2020 (Julian Date 303 2020). The yield was 0.9915 metric tons (991.5 kg) TNT-equivalent chemical explosion (based on 819.4 kg of C-4 and using a 1.21 TNT equivalency factor). Explosives dimensions were: 46.0” (L) x 37” (W) x 29.25” (H) (1.1557 m x 0.9398 m x 0.74295 m). Explosive height was 6.5 inches above the ground (on a plastic pallet) in an approximately 1 m deep crater with a diameter of approximately 4 m at the same location as Artemis. The UNR local seismic magnitude is M_L about 0.65. This is larger than the 0.43 of Artemis and may reflect some enhanced coupling due to the crater.

5 Far-Field Instrumentation

Three primary types of far-field sensors (seismic, infrasound, and weather) were deployed for the LSECE shots, as described in the following sections. The waveform sensor data in this data release used the Federation of Digital Seismograph Networks (FDSN.org) network code SN (Southern Great Basin Network). The far-field surface seismic range is differentiated from near-field surface and borehole seismic sensors by distance (i.e., 200 m from the source hole), which was approximately four times beyond the predicted elastic radii of the largest DAG experiment (<50 m). In the near field, high-shock accelerometers were required inside the zone of nonlinear hydrodynamic deformation, while the far field is considered a zone of linear-elastic deformation.

5.1 Surface Seismic Instrumentation

The primary set of far-field seismic data collected came from geophones and accelerometers in place for both LSECE shots. LSECE took advantage of the existing seismic network that was deployed for DAG with 95 percent of DAG array sensors operational. The other 5 percent were not telemetering properly and are not included in the data release. An additional set of data was collected from a grid of 496 closely spaced geophones (“Large N”) placed within 200 to 2,500 m of SGZ. The following sections provide information about the various seismic arrays

5.1.1 Accelerometers

POC: Bob White

The 22 accelerometers deployed around SGZ were arranged with a similar naming convention as the geophone rings (Figures 18 and 19). The Kinemetrics EpiSensor or EpiSensor2 force balance accelerometers were combined with RefTek 130S data acquisition systems. The naming convention for the rings included two numbers, the radii from SGZ (0.5km, 1.3km, 1.5km, and 2.0km as D5, D13, D15, and D20) followed by ‘M’ and a sequential number from 0 to 9 or A, clockwise from north. There were some gaps in sensor surface coverage due neighboring collapse craters created by previous historical underground nuclear explosions. The horizontal

geophone channels (CNR and CNT) were oriented toward the source hole in radial and transverse configurations, and vertical channel CNZ is oriented positive upward. Two accelerometers (U1AS and U1AU) located in Area 1 of the NNSS had horizontal components oriented in north-south and east-west configurations (CNN and CNE). The accelerometer sampling rates were 500 sps and Nyquist frequency 250 Hz. The exception was with stations U1AS and U1AU set to a rate of 250 sps.

5.1.2 Broadbands

The 26 broadband sensors were deployed around SGZ and within the NNSS boundary (Figure 21). Instrumentation included Nanometrics Trillium 120 Compact sensors and RefTek 130S or Kinemetrics Quanterra Q330 data acquisition systems. Four of these broadbands (I20M0, I20M3, I20M6, and I20M9) were within a 2-km geophone ring around SGZ. Some of the broadband sites from SPE Phase II (DAG) remained in place for LSECE, including three instruments place by AFTAC (AF001, AF004, and AF005), which are 3C triaxial force-balance PMD SP400U3 electrochemical transducers. The 3C broadband channels (CHZ, CHN, and CHE) were oriented in the standard seismology vertical, north-south, and east-west component configurations. Broadband channels were sampled using either 250 or 500 sps, resulting in Nyquist frequencies of either 125 or 250 Hz, respectively.

5.1.3 Large N Seismic Array

POC: Cleat Zeiler

A temporary seismic deployment consisting of a large number of geophones was installed for the DAG tests and utilized again in the LSECE shots. This array is commonly referred to as “Large N.” The Large N array includes 446 DT-SOLO 5 Hz 3C geophones that were deployed from October 22 – November 9, 2020. The array covers an area of approximately 2.5 km by 2 km, with a spacing of 100 m (Figure 1). Two dense lines with a spacing of 50 m are along the southwest and southeast direction. The distance from the geophones to the LSECE test location ranges from approximately 200 to 2,500 m.

Data recovery for the Large N seismic array is greater than 98%. The INOVA Acquisition Systems store data in a modified SEG-Y Rev. 0 format. Metadata, such as sensor locations, are all stored in the SEG-Y header. The locations are specified using UTM Zone 11 North coordinates. Channel 1 is vertical, channel 2 is east-west, and channel 3 is north-south. The microsecond part of the record time is stored in bytes 169–172. The sensitivity of the sensor is 80 Volts/meter/second.

292 geophones recorded at 1,000 sps, and 199 geophones recorded at 500 sps. The origin time for the data with 1,000 sps is 18:45:56.921 and the origin time for the data with 500 sps is 18:45:57.000. Seven stations did not record both events – 3/8, 4/8, 4/9, 11/12, 17/6, and 18/11. Station 20/18 channel 1 failed on Apollo.

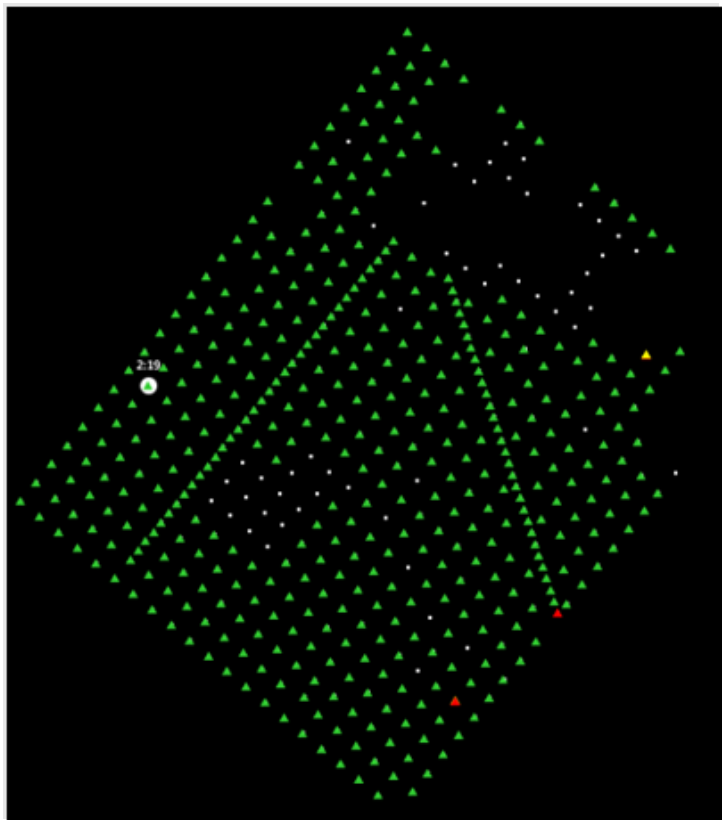

Figure 1: Layout of the large-N array relative to LSECE shots.

5.2 Infrasound Instrumentation

Infrasound instrumentation included 54 stations located from 1 to 16 km distance from the LSECE shots. The acoustic network was designed to capture a transect down Yucca Flat from near the source to beyond the distance where lower atmospheric structure begins to affect sound propagation. Additional sensors were deployed radially at two different ranges to capture direction-dependent infrasound radiation. Two 8-element subarrays were deployed at a range of about 5 km from GZ, one to the north and one to the west. These stations consisted of sensors inherited from the DAG network, as well as additional equipment contributed by ARA (section 5.2.1) and DTRA (section 5.2.2). The dynamic range of the sensors were adjusted based on proximity to GZ, but even with this precaution some of the data are clipped. In addition, some sensors failed between deployment and the LSECE events, which was not discovered until afterwards due to the lack of real time telemetry. The deployments are shown in Figure 2. Data for all deployments are stored in SAC format, covering the period of October 27 00:00:00 UTC to November 8 00:00:00 UTC 2020.

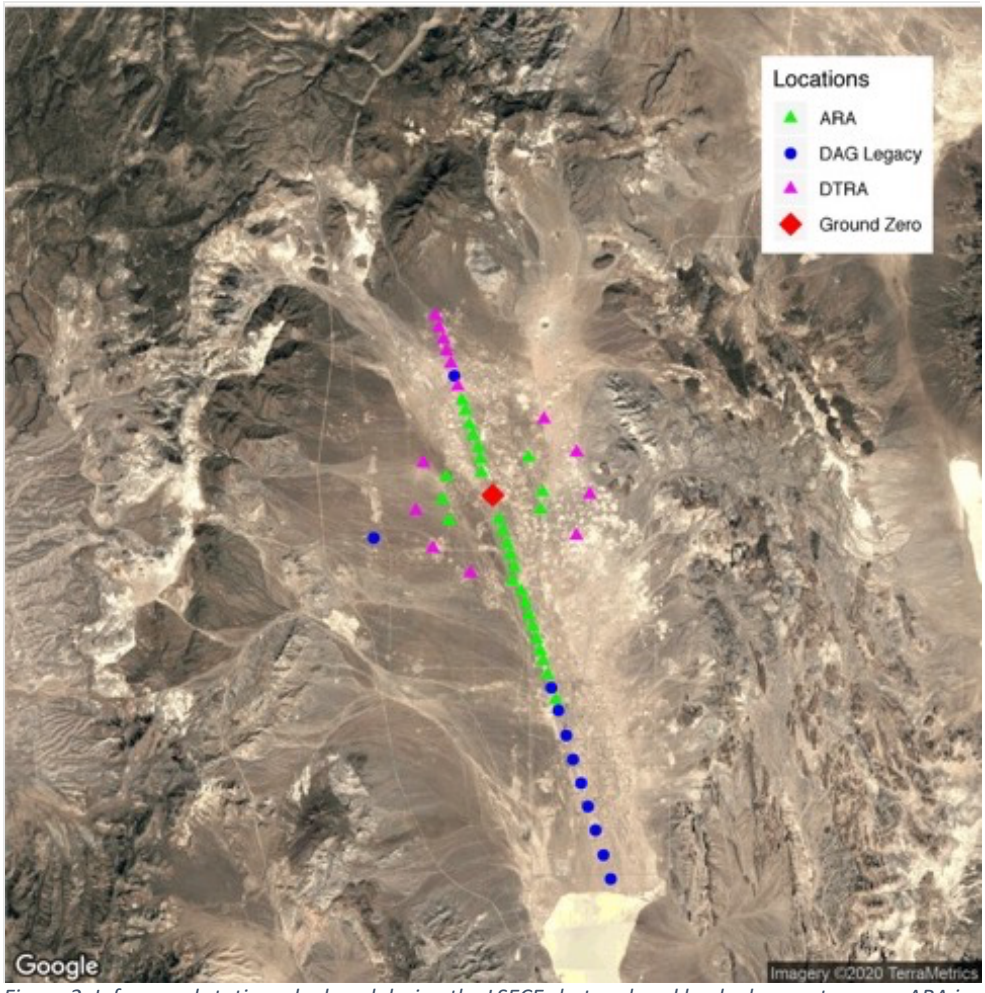

Figure 2: Infrasound stations deployed during the LSECE shots colored by deployment source. ARA is shown in green triangle, DTRA in magenta triangle, legacy DAG in blue circle, and GZ in red diamond.

5.2.1 ARA Deployment

POC: Mark Leidig

ARA installed a linear profile from 4 km north of GZ to 8.5 km south of GZ consisting of 22 of the 54 deployed infrasound stations. The stations are shown as green triangles in Figure 2. Stations were named with the direction and distance multiple by 10 (e.g. S045 is at 4.5 km south of GZ). An additional 8 stations were deployed in a ring at 2 km distance from GZ. These were the same from the DAG experiment. Detailed information on the instrumentation, configuration, and instrument response can be found in Attachment 1.

Ninety-eight percent of the data was successfully recovered from the sensors. Of the 30 sensor sites and two LSECE shots, only one measurement is not available due to a hardware issue. The event data are provided in SAC format. The files use the following filename convention: Event_Station_Network_LocationCode_Channel.sac

An example file name is Apollo_I20M9_WG_02_FDF.sac where Apollo is the event name, I20M9 is the station, WG is the network, 02 is the location code defining the hardware configuration (Table 2 of Attachment 1, Appendix A), and FDF is the channel name.

5.2.2 DTRA Deployment

DTRA deployed 14 of the 54 deployed infrasound stations. The DTRA stations are shown in pink triangles in Figure 2. The station names and configurations are described in Table 2. One hundred percent of the data was recovered from all 14 stations. The data was of overall good quality. One station had higher noise levels for Artemis that was not present during Apollo. Even so, the station was usable. There were data gaps throughout the deployment due to either system being temporarily powered down for maintenance or system unexpectedly being powered down due to low battery or another malfunction. No data gaps coincided with Artemis and Apollo.

Stations	**Instrument**	**Sensitivity**	**Conversion Factor**
N050, N055, FL793, FL791, FL781, FL786	NT Hyperion H2 Gages	1000 Pa	0.000112819 Pa/count
N060, N065, N070, N075	Hyperion H1 Gages	100 Pa	0.000112819 Pa/count
FL792, FL790, FL785, FL787	Validyne Gages	0.125 psi (~862 Pa)	0.00027 Pa/count

Table 2: DTRA acoustic deployment instrumentation calibration information. All stations were recorded on Reftek 130s digitizers.

5.2.3

5.2.4 Airborne Infrasound

POC: Daniel Bowman

5.2.4.1 Artemis

One helium balloon was launched for Artemis. The balloon had one payload with three channels: a prototype condensor microphone (CDF1), reversed-polarity infraBSU (channel CDF2), and a normal-polarity infraBSU (channel CDF3). The package also contained an Android cellphone running the RedVox infrasound recording app. The prototype condensor microphone was provided by Jake Anderssen at Boise State University (BSU). Further iterations of this design are now called the Camas sensor. The infraBSU polarity reversal is accomplished by swapping the position of the mechanical filter. This assists in determining whether recorded waveforms are "true" pressure signals as opposed to electronic interference or internal interference (see Equation 1 in Bowman and Lees (2018). InfraBSU microphones are described in Marcillo et al (2012). They were digitized on DiGOS DATA-CUBE logger.

Data was recovered from the payload and a potential arrival from Artemis was observed in the data. The data is recorded in SAC format as yyyy.ddd.hh.mm.sss.sta.chan.SAC. The station name for this balloon payload was B1HI. An example data file is 2020.306.15.00.00.B1HI.CDF1.SAC.

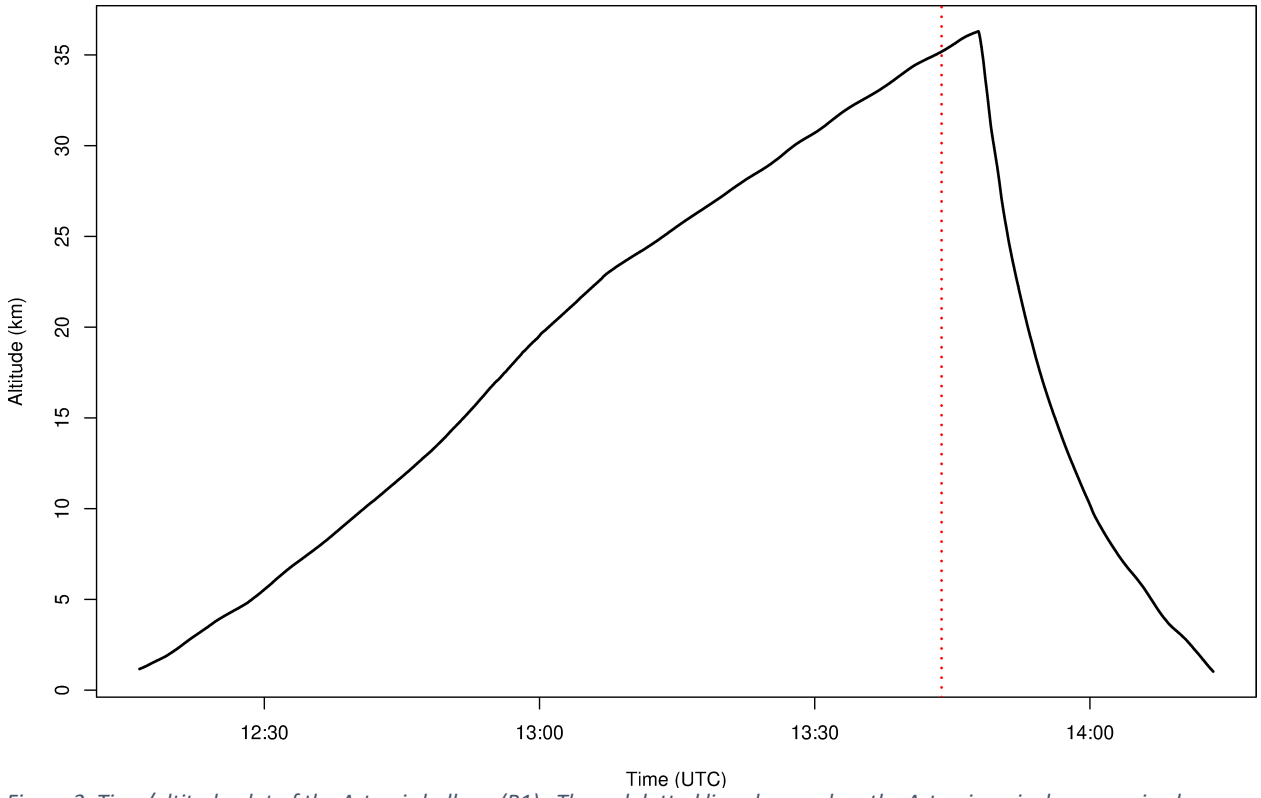

Figure 3: Time/altitude plot of the Artemis balloon (B1). The red dotted line shows when the Artemis arrival was received.

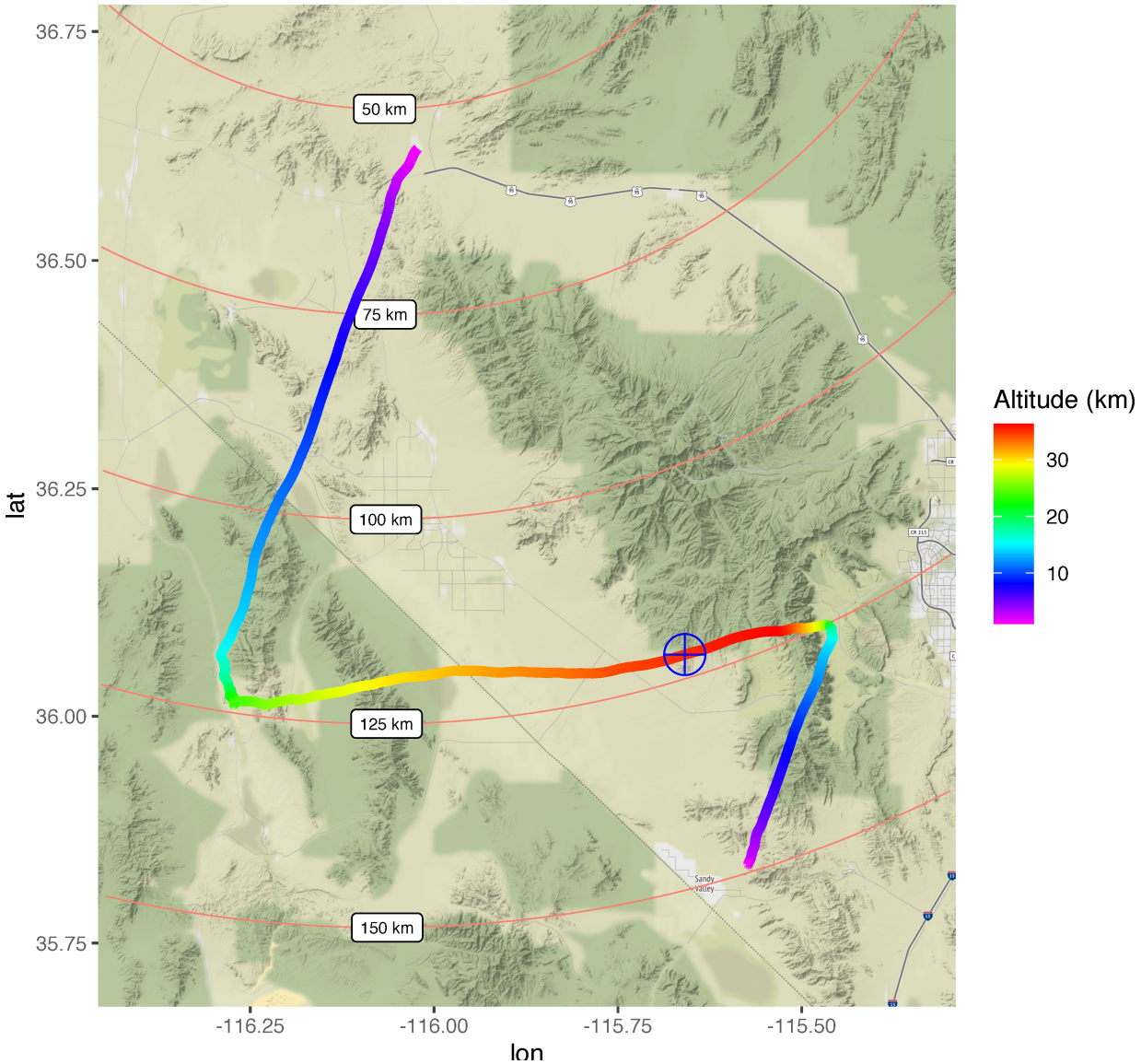

Figure 4: Trajectory of the Artemis infrasound balloon (B1), launched from Desert Rock Airport.

5.2.4.2 Apollo

Four solar hot air balloons (Bowman et al., 2020) were launched for Apollo. Balloon 2 carried the recovered payload from Balloon 1 during Apollo. Therefore, the channels are configured the same way: a prototype condenser microphone (CDF1), reversed-polarity infraBSU (channel CDF2), and a normal-polarity infraBSU (channel CDF3). An android cellphone running the RedVox infrasound app was also included. Balloon 3 contained two payloads both with a Gem microbarometer (Anderson et al., 2018). The lower payload (B3LO) was approximately 300ft below the upper payload (B3HI). Balloon 4 (B4HI) had a 700 ft reel, but the bottom package was lost on impact. Therefore, only one data channel (the upper package) is available. Balloon 5 (B5HI) had a single payload with a Gem microbarometer and an Android cellphone running the RedVox infrasound app.

Balloon 2 payload landed by the time Apollo was fired and thus did not record the shot while in air. Balloon 3, 4, and 5 all recorded Apollo shot while in flight. All Gem microbarometers in flight during Apollo recorded a clear signal, but the cellphone on Balloon 5 had run out of batteries before the event. Similar to Balloon 1, the data is recorded in SAC format as yyyy.ddd.hh.mm.sss.sta.chan.SAC.

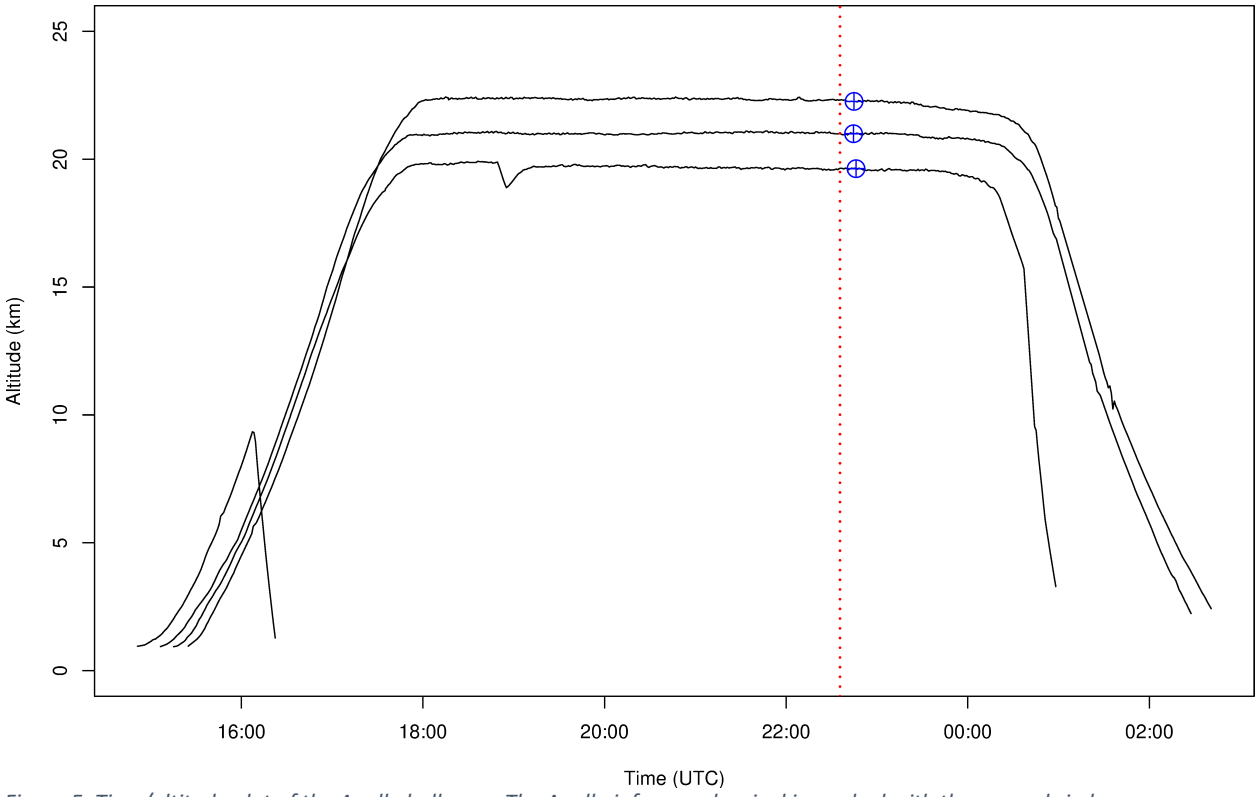

Figure 5: Time/altitude plot of the Apollo balloons. The Apollo infrasound arrival is marked with the crossed circle.

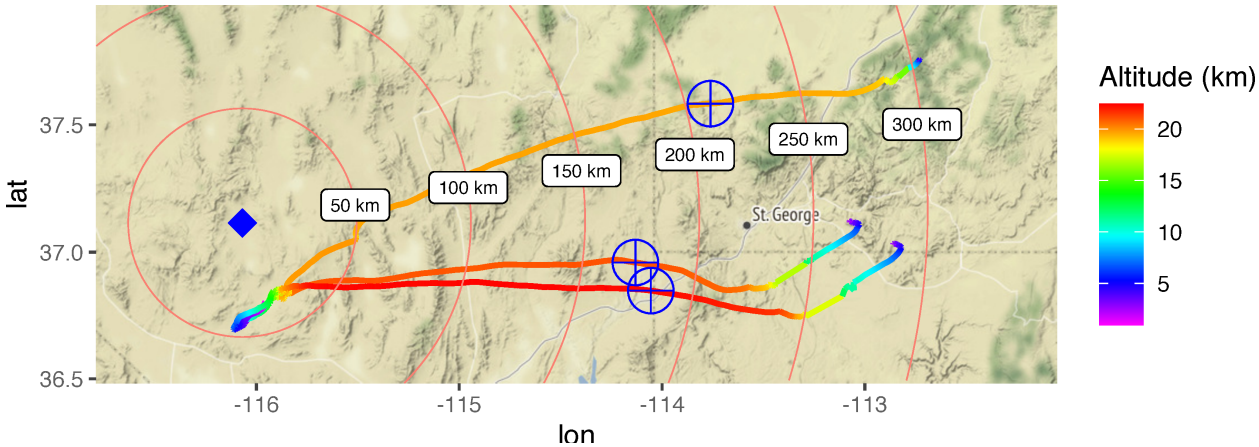

Figure 6: Trajectories of the Apollo balloons. The location of the balloons when the infrasound arrival was captured is marked with crossed circles.

5.3 Weather Instrumentation

POC: Walter Schalk

Weather data were collected for LSECE to provide information needed for analysis of surface acoustic measurements such as infrasound. Weather data for the tests were collected from six semi-permanent stations in the network of weather stations managed by the NNSS Weather Operations, Air Resources Laboratory/Special Operations and Research Division (ARL/SORD). This network is known as the SORD/NNSS Weather Mesonet, and consists of 24 stations located across the NNSS. The design of a mesonet station is shown in Figure 7 and station locations in Figure 8.

At each of the six stations, wind and other weather observations, including temperature, humidity, atmospheric pressure, and solar radiation, were taken to provide 15-minute averaged data. Data is provided in individual station excel sheets with a listing of the 15-minute averaged data collected every 15 minutes.

Detailed information about the weather data collection can be found in Attachment 2.

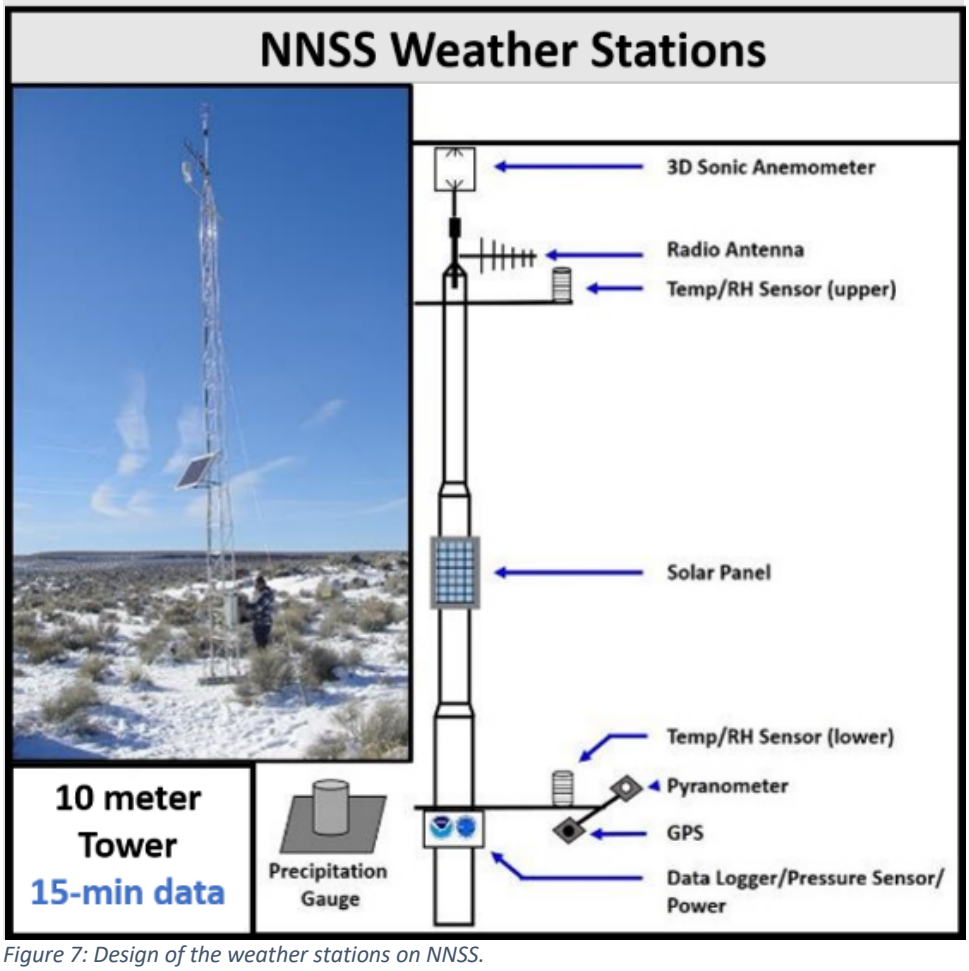

Figure 7: Design of the weather stations on NNSS.

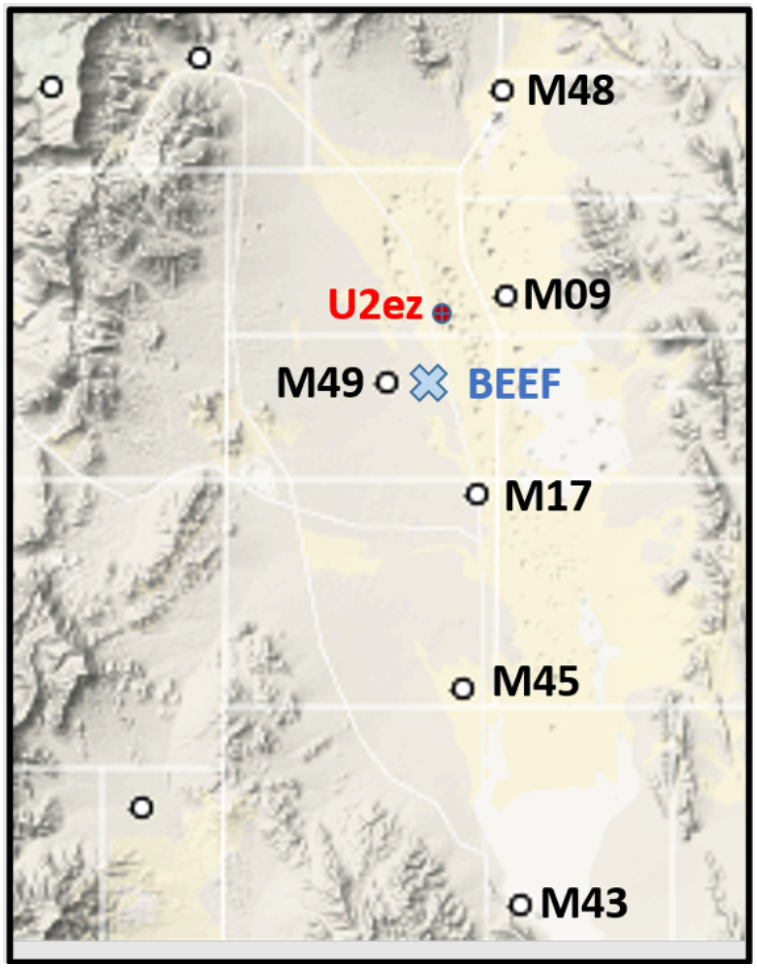

Figure 8: Location of the six NNSS weather stations (M##).

6 Near-Field Instrumentation

6.1 Borehole Accelerometers

POC: Zack Cashion and Bob White

LSECE utilized the twelve DAG legacy boreholes. Each package consisted of a 3C accelerometer, with triaxial sets mounted 120 degrees apart on the same radius. All ranged a minimum of three times the maximum predicted acceleration. They had a minimum 5,000 g shock survival rating. The Z axis was oriented upward, and the X and Y axes are orthogonal to Z. The borehole locations are shown in Figure 9.

The LMS and Pacific systems triggered properly with no issues seen in the data. The LMS data is provided in MatLab files, while the Pacific systems are in csv format. MatLab is required to read the LMS system waveforms.

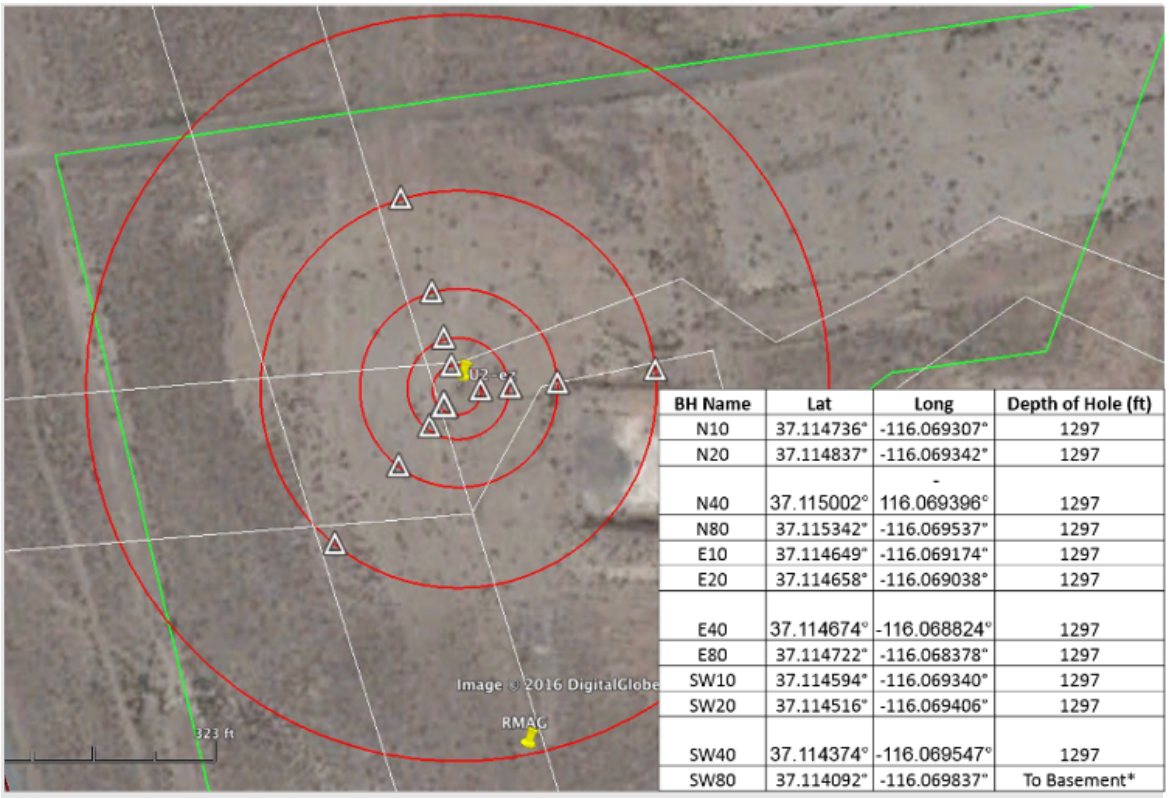

BH Name	Lat	Long	Depth of Hole (ft)
N10	37.114736°	-116.069307°	1297
N20	37.114837°	-116.069342°	1297
N40	37.115002°	-116.069396°	1297
N80	37.115342°	-116.069537°	1297
E10	37.114649°	-116.069174°	1297
E20	37.114658°	-116.069038°	1297
E40	37.114674°	-116.068824°	1297
E80	37.114722°	-116.068378°	1297
SW10	37.114594°	-116.069340°	1297
SW20	37.114516°	-116.069406°	1297
SW40	37.114374°	-116.069547°	1297
SW80	37.114092°	-116.069837°	To Basement*

Figure 9: Legacy DAG borehole accelerometer locations in white triangles.

6.2 Near-Field Surface Accelerometers

POC: Zack Cashion and Bob White

A near-field surface accelerometer array of 6 stations was installed in the same locations as DAG, within 200 m of the U-2ez source hole, to capture the extent, if any, of surface spall and supplement the near-field high-shock accelerometers in satellite boreholes. At the surface, accelerometers were installed in six lines radiating out from the surface location of SGZ, spaced at 60-degree increments azimuthally. Three of the units collected data continuously at 2KHz from October 22-29, 2022. The other three units collected triggered data over the same period and sampling rate.

7 Additional Diagnostics

7.1 Distributed Acoustic Sensors

POC: Robert Abbott

DAS technology was deployed for the LSECE experiments in an effort to track continuous wavefields in addition to the few widely spaced point measurements, available from typical geophone layouts. The DAS deployed is a fiber-optic sensing system comprising an advanced optoelectronics interrogator and sensing cables. Helically-wound fiber cable (HWC) placed in two boreholes in vertical seismic profiling configurations recorded up-going and down-going P and S waves. The LSECE DAS deployment was consistent with what was done for the DAG deployment which is described below.

Three Silixa Carina interrogators were in place and recorded DAS data for both LSECE shots. Interrogators 1 and 2 were attached to HWC with 30-degree pitch. Both HWC fiber runs start at a junction box located between instrumentation holes SW80 and E80. Interrogator 1 was run southwest from the box and inserted into borehole SW80, and interrogator 2 was run northeast from the box and inserted into borehole E80. Interrogator 3 was attached to BEEF Trailers straight (i.e., not HWC) Silixa Constellation fiber that extended southeast from the surface junction box to the recording station over 2 km away. All surface fiber was installed in a trench up to 15 centimeters below ground surface and backfilled with native material. The downhole portions were grouted in place. Figure 29 shows a map showing the layout of the fiber optic cable lines.

The gauge length of the interrogators was 2 m (7 ft). The sample rate depended on the interrogator and the experiment, and ranged from 36 to 100 kilohertz (kHz). Full sample-rate data are not available. All data were exported by the vendor at 2,000 Hz.

There was some loss of data due to fiber damage (~100 out of 2400). Data from interrogators 1 and 2 were combined into a single SEG-Y file per experiment (file has 'HWC' in filename). Data from interrogator 3 are in a separate SEG-Y file per experiment (data have 'surface' in filename). The SEG-Y files were exported from Schlumberger Vista software and are in a Floating-Point IBM format. An effort was made to conform to SEG-Y Revision 1 standards, but some header variables may not strictly adhere. The data are in units of strain rate: nanometers/meter/second. All source and receiver locations are reported in the SEG-Y headers in UTM Zone 11 North and elevations are in WGS84 meters.

7.2 Magnetometers

POC: Bob White

Similar to other instrumentation, the magnetometer deployments were the same from DAG to LSECE. More background information is provided in MSTS LLC 2021. Two setups, at distances of 30 and 60 m (horizontal distance from SGZ), were installed (Table 3). Each setup consisted of three orthogonal B field sensors (EMI BF-5/6 magnetometers) with coil windings and a nominal response of 1–100 kHzFigure 10. A seismic sensor, typically a KMI EpiSensor, was installed at each location as well, to measure ground motion, because the arrival of the seismic wave will produce signals due to the motion of the sensor within the Earth's magnetic field. A seismic sensor is essential for proper interpretation of the data (e.g., Sweeney 2011) and to ensure that that signal associated with later-arriving ground motion can be distinguished from the actual source EM signal, which arrives earlier due to higher propagation speed of the EM signals (~3e10 m/s) as opposed to the seismic signals (~3e4 m/s).

Data were recorded on a six channel Reftek at 500 or 1000 sps. The Reftek uses a non-causal finite impulse response (FIR) anti-alias filter, which may produce acausal transients for high-frequency signals near the Nyquist frequency. The exact response of the FIR differs with the firmware version. Timing is based on a crystal oscillator with periodic locks to an external GPS signal.

No data was recorded on the 30m site for Artemis since there was no interface box. Additionally the 30m site had clock timing issues.

Station	Digitizer SN	Latitude	Longitude	Elevation (m)
EM - 30m	B258	37 13 14.69	116 03 40.29	1520
EM - 60m	B259	37 13 13.72	116 03 40.80	1523

Table 3: Electromagnetic station locations.

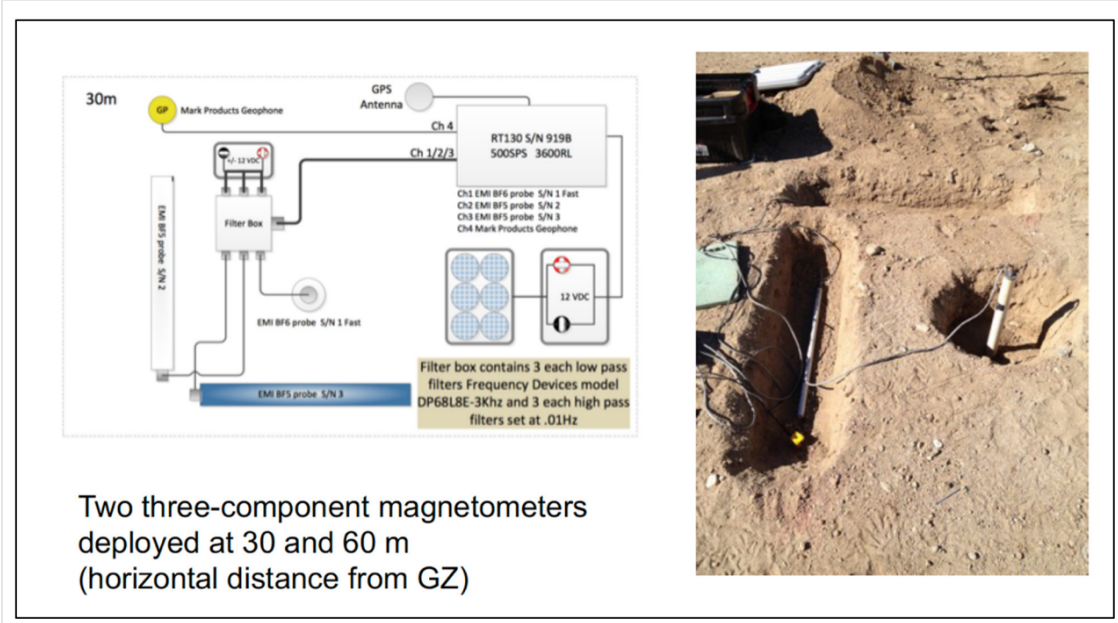

Figure 10: Magnetometer setup shown in left image. Right image shows co-located magnetometer and episensor.

7.3 Video

7.3.1 High Speed Video Cameras and HandiCams

POC: Bob White

MSTS fielded one high-speed Phantom V711 cameras and twp handy cams for each of the LSECE shots. The goal of fielding both high-speed and low-speed video was to capture any ground motion, determine estimates of shock propagation, determine symmetry of shock propagation, and also record any late-time events that may have occurred at the test bed and the surrounding area from different vantage points. The high-speed video camera was looking ENE relative to the shots, while the handy cams were looking NE and SE. The high-speed camera was in a large enclosure (known as the “Ice Box”) which was temperature controlled and had a viewpoint on the side covered by plexiglass so no wind or debris would interrupt the view of the camera. It also housed all of the equipment necessary to communicate with the systems remotely from the BEEF trailer park. In order to mitigate any sort of ground vibration coming from the equipment so it would not affect the seismic recording equipment, all of the equipment in the Ice Box trailer were running either off of a RUPS unit or dedicated battery supplies for the high-speed camera.

7.4 Unmanned Aerial System (UAS) Photogrammetry

POC: Margaret Townsend

The low-altitude aerial photogrammetry diagnostic was designed to capture high-resolution overhead imagery with surface ground control in order to develop detailed topographic models before and after Apollo and Artemis. This diagnostic involved the deployment of a commercial-off-the-shelf digital single-lens reflex (DSLR) camera, fixed to a small unmanned aerial vehicle and deployed at low altitude (<40 m above ground level). The vehicle plus the sensor is referred to as an unmanned aerial system (UAS). Imagery was collected in a pre-defined boustrophedonic pattern over a region of 820 m by 720 m (~3,160 m2). During Artemis, the camera system failed and minimal photos were captured. During Apollo, the GPS system failed and the flight was canceled. As a result, no UAS photogrammetry data was captured nor provided in this data release.

8 Summary

This report describes the official release of sensor data recorded from the two ground surface chemical explosions carried out by the DTRA sponsored LSECE project in October 2020.

9 References

Jacob F. Anderson, Jeffrey B. Johnson, Daniel C. Bowman, Timothy J. Ronan; The Gem Infrasound Logger and Custom-Built Instrumentation. Seismological Research Letters 2017;; 89 (1): 153–164. doi: https://doi.org/10.1785/0220170067

Bowman,D.C.,&Lees,J.M.(2018). Upper atmosphere heatingfrom ocean-generated acousticwave energy.GeophysicalResearch Letters,45, 5144–5150.https://doi.org/10.1029/2018GL077737

Bowman, D. C., Norman, P. E., Pauken, M. T., Albert, S. A., Dexheimer, D., Yang, X., Krishnamoorthy, S., Komjathy, A., & Cutts, J. A. (2020). Multihour Stratospheric Flights with the Heliotrope Solar Hot-Air Balloon, Journal of Atmospheric and Oceanic Technology, 37(6), 1051-1066.

List of Attachments

1. Leidig, M., 2022. Written communication prepared by the Weston Geophysical Group, Applied Research Associates. Large Surface Explosion Coupling Experiment: Excerpts from ARA Quick Look Report on Acoustic Data Measurements.
2. Schalk, W., 2020. Written Communication prepared by the NNSS Weather Operations, Air Resources Laboratory/Special Operations and Research Division. LSECE and BEEF Weather Data Collection. Mercury, NV.

Attachment 1

Leidig, M., 2022. Written communication prepared by the Weston Geophysical Group, Applied Research Associates. Large Surface Explosion Coupling Experiment: Excerpts from ARA Quick Look Report on Acoustic Data Measurements.

Large Surface Explosion Coupling Experiment: Excerpts from ARA Quick Look Report on Acoustic Data Measurements

Version: N/A

Original Document Date:
18 December 2020

Excerpts Document Date:
03 August 2022

Funding Provided by:
Defense Threat Reduction Agency

Prepared by:
Mark Leidig
Weston Geophysical Group
Applied Research Assoc.
mleidig@ara.com

Table of Contents

©2022 Applied Research Associates, Inc. (ARA)

All contents subject to the warning(s) on the title page of this document.

List of Figures

©2022 Applied Research Associates, Inc. (ARA)
All contents subject to the warning(s) on the title page of this document.

List of Tables

©2022 Applied Research Associates, Inc. (ARA)
All contents subject to the warning(s) on the title page of this document.

1. Diagnostic Hardware

Acoustic

ARA installed acoustic sensors to provide linear and azimuthal measurements of the above ground Large Surface Explosion Coupling Experiment (LSECE) explosions. Figure 11 shows the locations of these sensors relative to the ground zero (GZ) detonation point. ARA installed a linear profile from 4 km north of GZ to 8.5 km south of GZ consisting of 22 stations at 0.5 km spacing. We named stations with the direction and distance multiplied by 10 (e.g. S045 is at 4.5 km south of GZ). A ring at 2 km distance from the LSECE GZ consisted of 8 stations, and we used existing station names from the Dry Alluvium Geology experiment.

ARA utilized Hyperion IFS-5000 series seismically decoupled infrasound sensors with varying peak pressure limits. The Hyperion IFS-5300 acoustic sensor with the high frequency shroud has a flat response between 0.01 and 100 Hz. With the poles and zeros provided in Table 4, a user can correct the data to have a flat response between 0.001 and 1000 Hz.

We recorded the data at 1000 samples per second (sps) with a gain of 1 on RefTek (130, 130S, and Wrangler) and Hyperion digitizers. Table 5 in Appendix A provides hardware configuration and values to convert raw data from counts to pressure (Pascals). Appendix B lists the operation dates for each station. We swapped the sensor at three ring sites prior to Artemis to allow on-scale recording of other nearby tests.

Figure 12 shows an example ARA station (not from LSECE) with an enclosure (holding the digitizer, GPS clock, battery, and charge controller), a solar panel, and a wind noise reduction dome covering the infrasound sensor. ARA stations at 2 km and greater distance, except the 2 km ring, utilized a Hyperion noise reduction dome. We placed the sensor on the ground without a dome along the 2 km ring and other stations closer than 2 km distance.

Table 4. Hyperion IFS-5300 Poles and Zeros.

ZEROS	**3**
0.0	0.0
0.0	0.0
0.0	0.0
POLES	**3**
-0.000848	0.0
-0.011300	0.0
-0.078500	0.0
CONSTANT	**1**

©2022 Applied Research Associates, Inc. (ARA)

All contents subject to the warning(s) on the title page of this document.

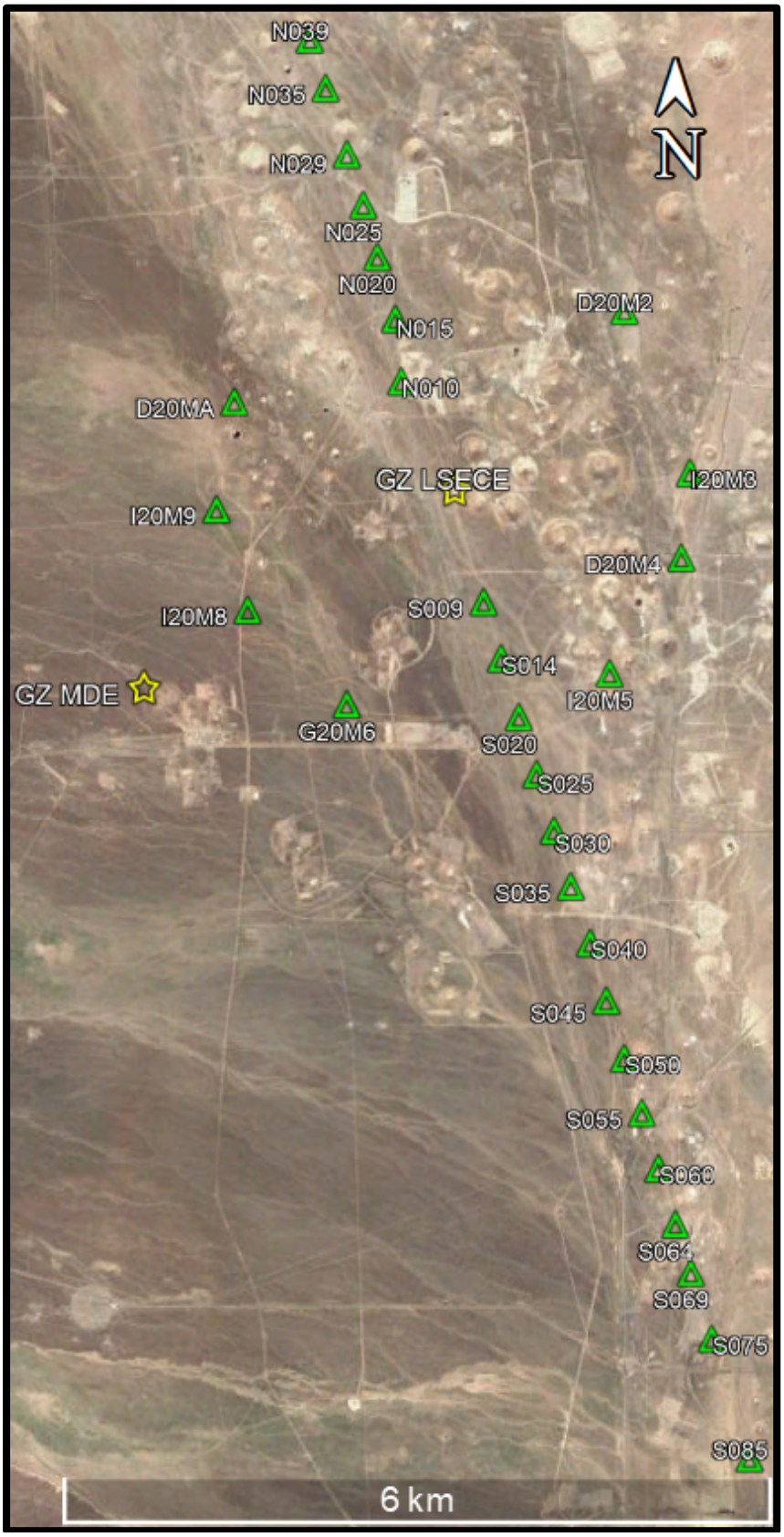

Figure 11. Satellite image showing ARA deployed acoustic sensors for LSECE. Green triangles mark the ARA sensor sites with a ring at 2 km distance and a linear array from 4 km to the north to 8.5 km to the south of the LSECE GZ. Google Earth background image.

©2022 Applied Research Associates, Inc. (ARA)

All contents subject to the warning(s) on the title page of this document.

Figure 12. Example of an ARA installation with electronics enclosure, solar panel, and wind noise reduction dome visible. The acoustic sensor is below the dome. Note: due to photographic restrictions on the NNSS, this installation is from an unrelated project and is not an actual LSECE installation.

2. Data

Data can be requested from Applied Research Associates (Mark Leidig; mleidig@ara.com). Acoustic data are available in miniseed format for raw, continuous data and Seismic Analysis Code (SAC) for the processed, cut data. The raw data are in counts as recorded by the digitizer. The processed data units are converted to Pascals using the values provided in Appendix A, Table 5. No response corrections were applied, and except for a trend removal, the processed data can be converted back to the original units in counts, if so desired.

As of December 2020, the cut data are located on the Univ. of Nevada-Reno data server in:
/disk1/home/bowmand/LSECE/raw/ara

The raw, continuous data are located on the Univ. of Nevada-Reno data server in:
/disk3/home/leidigm/LSECE_Data/Acoustic

Database Structure

The raw miniseed data are in year/day_of_year directory structure (e.g. 2020/303 for 10/29/2020). Files are named with the start time and convention:
StationName_Network.LocationCode.Channel.Year:DayofYear:Hour:Minute:Second
Example - N039_WG..1.2020:303:03:00:00

The cut data in SAC format are organized by event directories. An example of the data file naming format is:
Apollo_I20M9_WG_02_FDF.sac
where Apollo is the event, I20M9_WG is the station_network, 02 is the location code defining the hardware configuration (Table 5 of Appendix A), and FDF is a code name for the instrumentation and sample rates. FDF is a long period (≥ 10 s) pressure sensor recorded at 1000 samples per second or higher. All ARA sensors were recorded at 1000 samples per second.

©2022 Applied Research Associates, Inc. (ARA)

All contents subject to the warning(s) on the title page of this document.

3. Data Examples and Initial Observations

ARA successfully recovered over 98% of the LSECE test data from its sensors. Of the 30 sensor sites and two LSECE shots, only one measurement is not available due to a hardware issue. This report section provides images of the processed waveforms and a brief description of the data issue.

Signal Waveforms

The following plots show the ARA LSECE recordings converted to units of Pascals (Pa) and zoomed around the overpressure arrivals of both explosions. Figure 13 through Figure 34 show waveforms from north (N039) to south (S085). Figure 35 through Figure 42 show waveforms from the 2 km ring starting NE of GZ and moving clockwise.

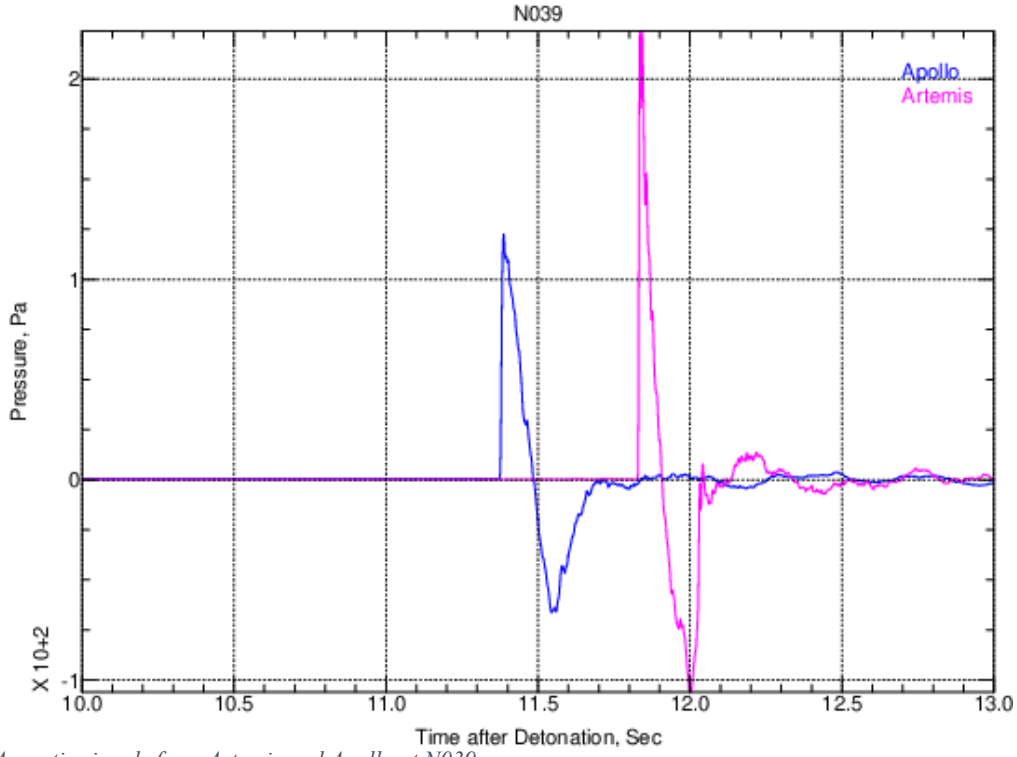

Figure 13. Acoustic signals from Artemis and Apollo at N039.

©2022 Applied Research Associates, Inc. (ARA)

All contents subject to the warning(s) on the title page of this document.

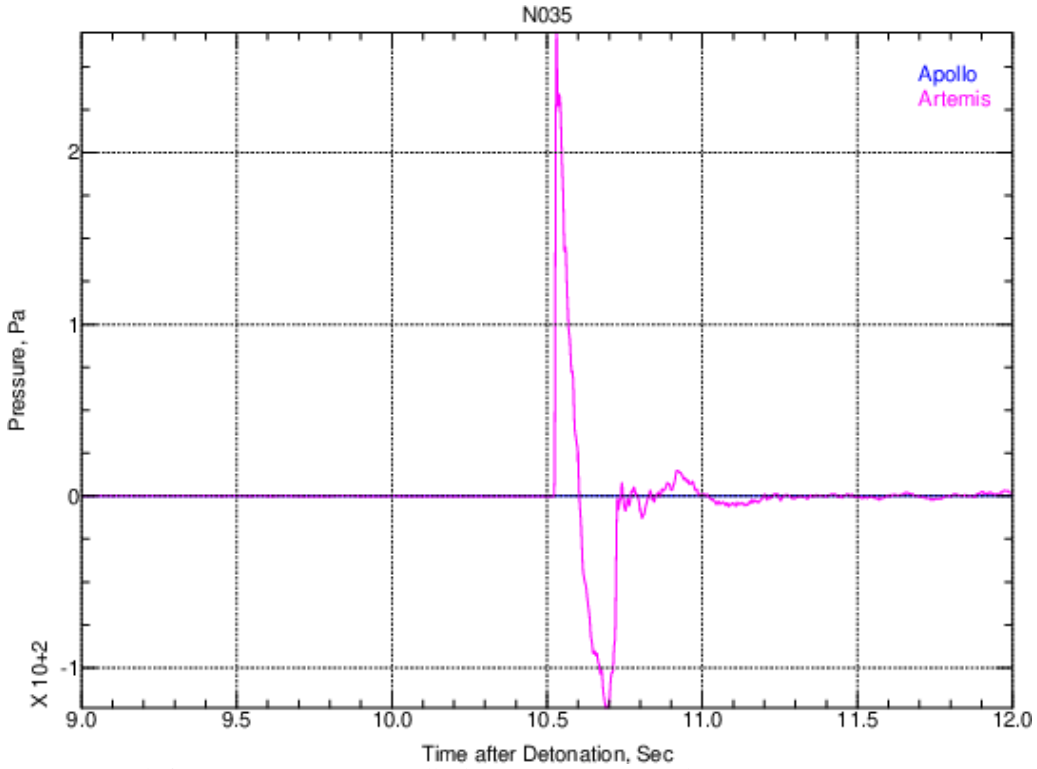

Figure 14. Acoustic signals from Artemis at N035. Apollo data were not recovered.

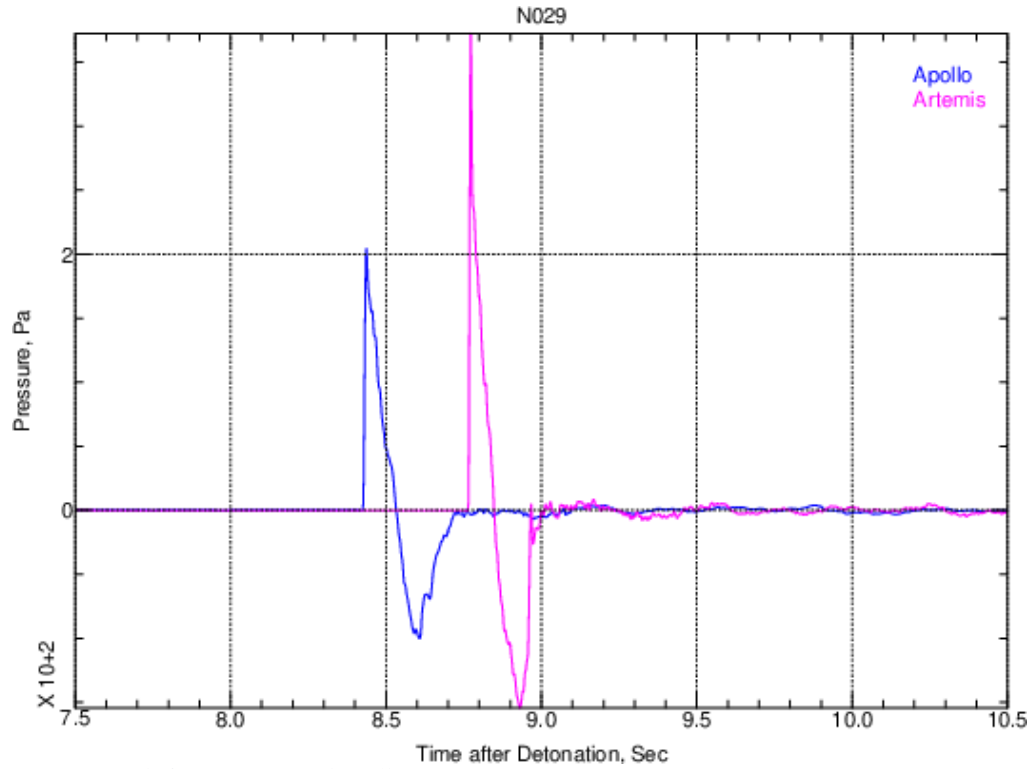

Figure 15. Acoustic signals from Artemis and Apollo at N029.

©2022 Applied Research Associates, Inc. (ARA)

All contents subject to the warning(s) on the title page of this document.

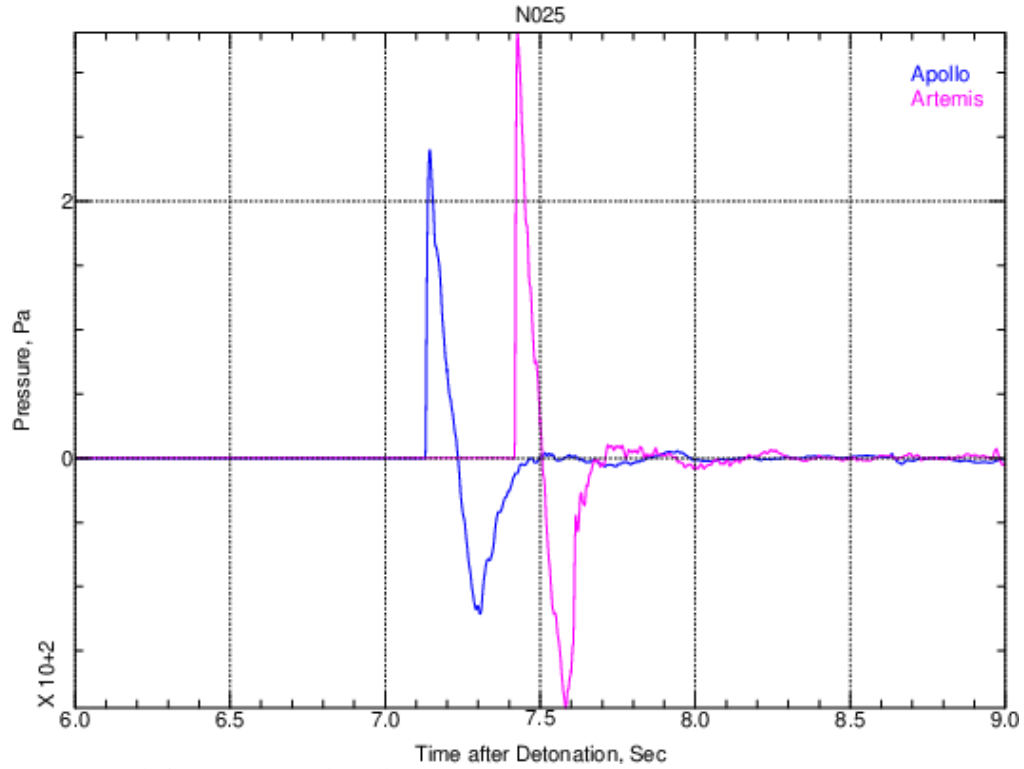

Figure 16. Acoustic signals from Artemis and Apollo at N025.

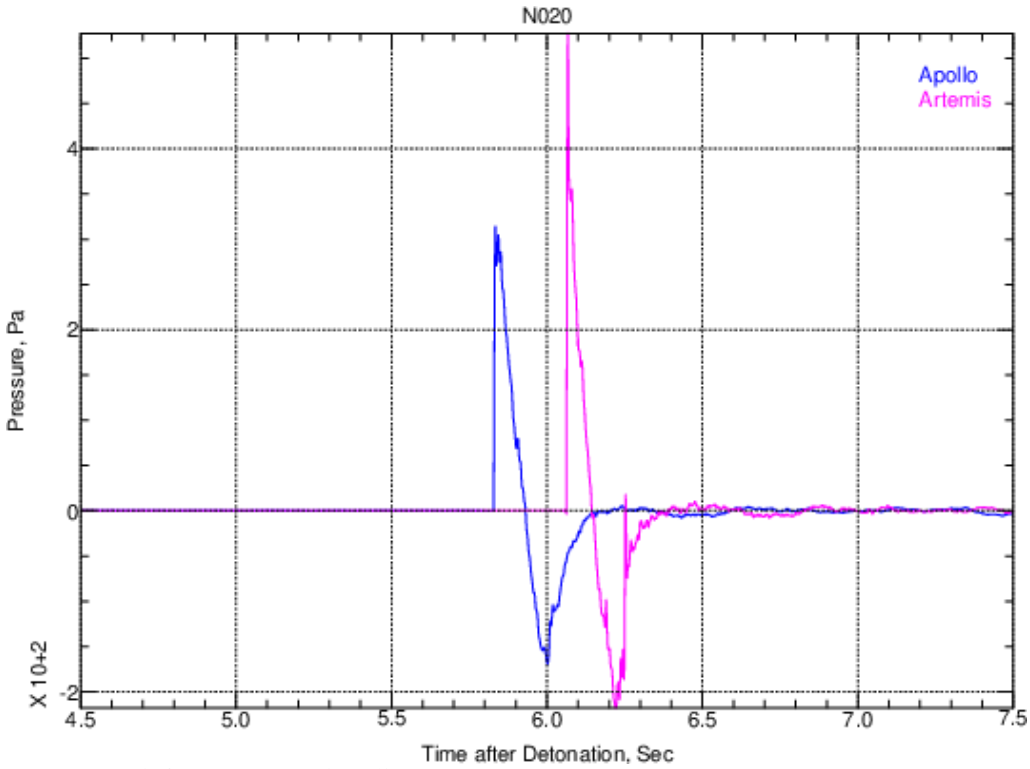

Figure 17. Acoustic signals from Artemis and Apollo at N020.

©2022 Applied Research Associates, Inc. (ARA)

All contents subject to the warning(s) on the title page of this document.

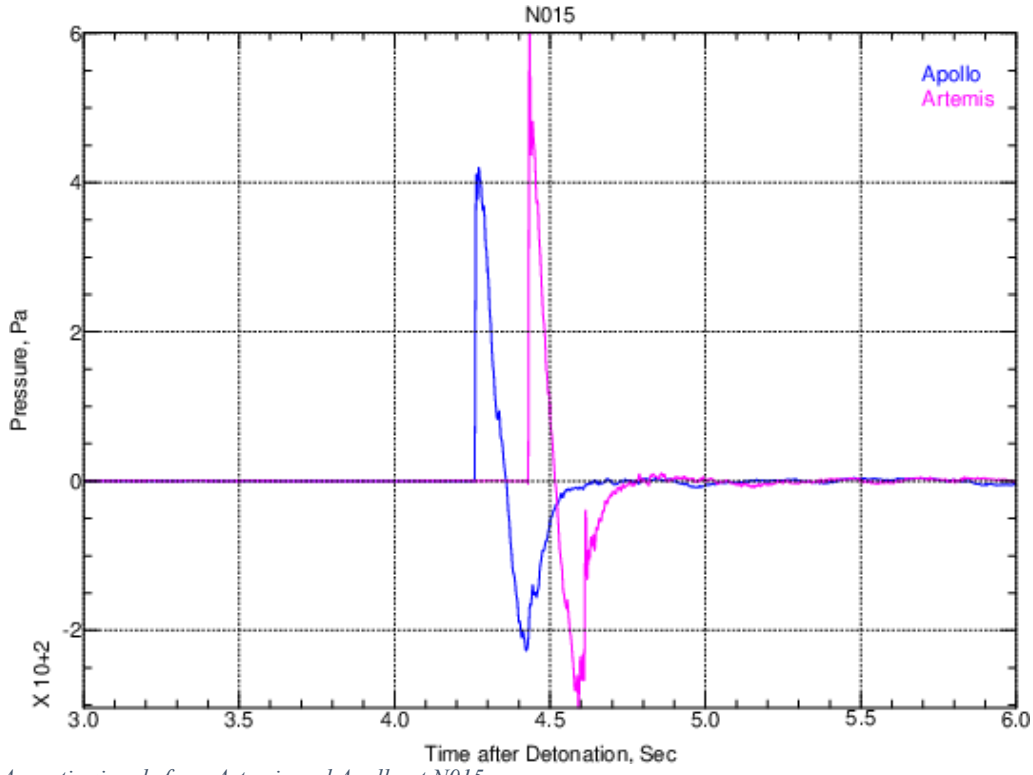

Figure 18. Acoustic signals from Artemis and Apollo at N015.

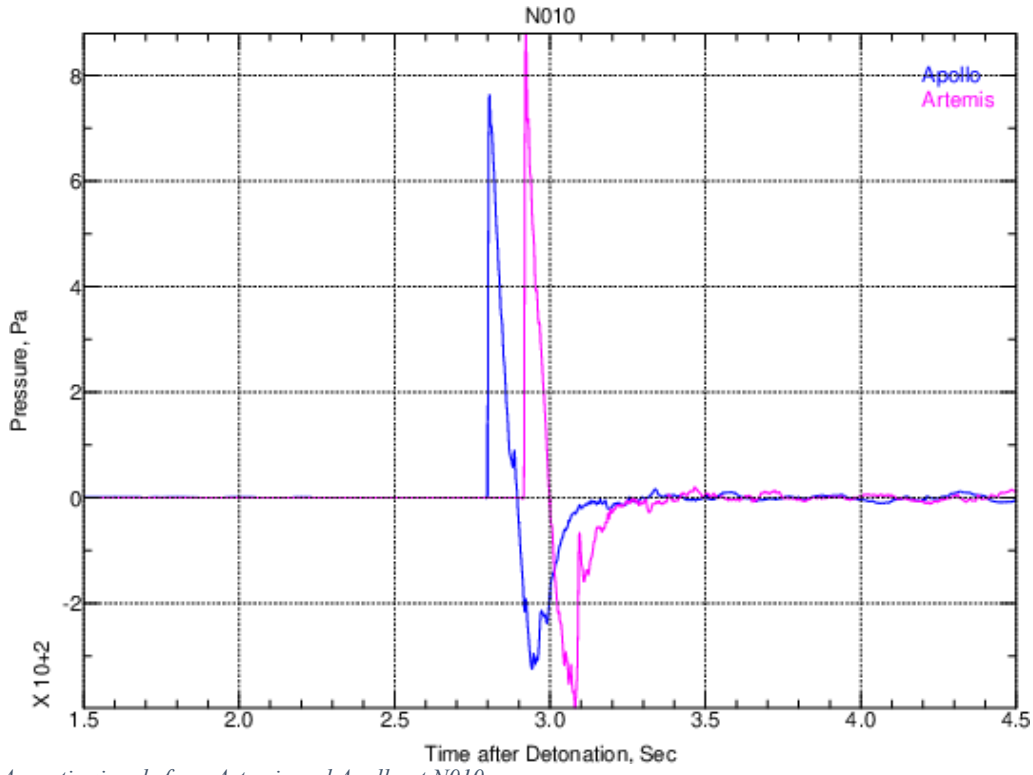

Figure 19. Acoustic signals from Artemis and Apollo at N010.

©2022 Applied Research Associates, Inc. (ARA)

All contents subject to the warning(s) on the title page of this document.

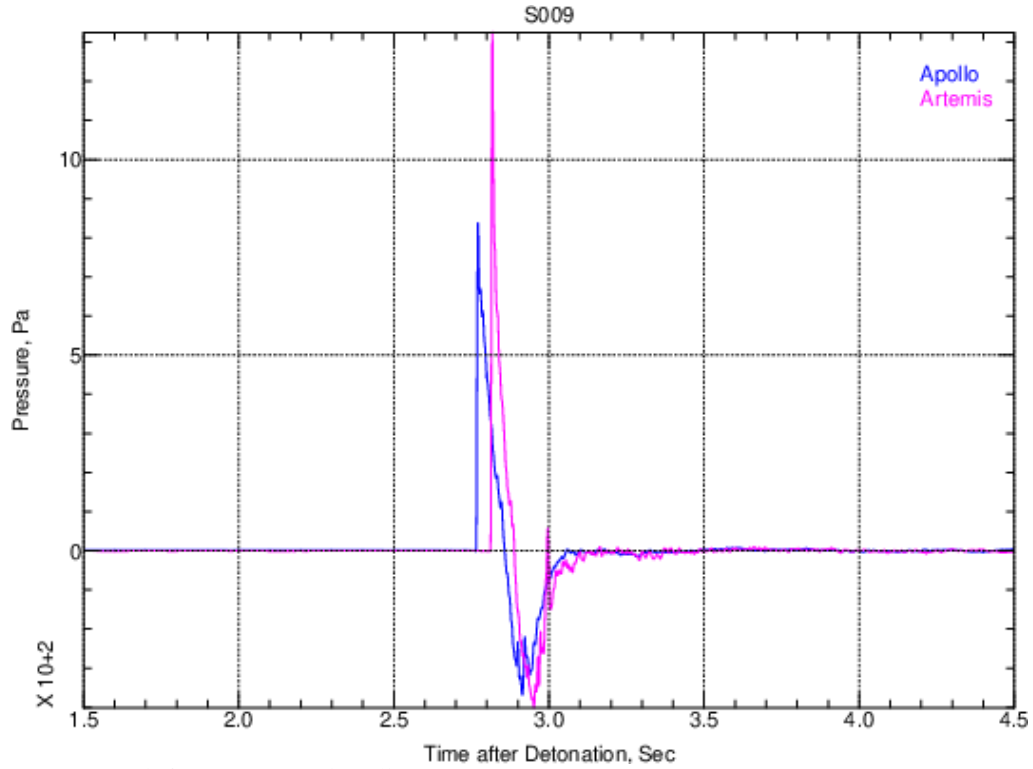

Figure 20. Acoustic signals from Artemis and Apollo at S009.

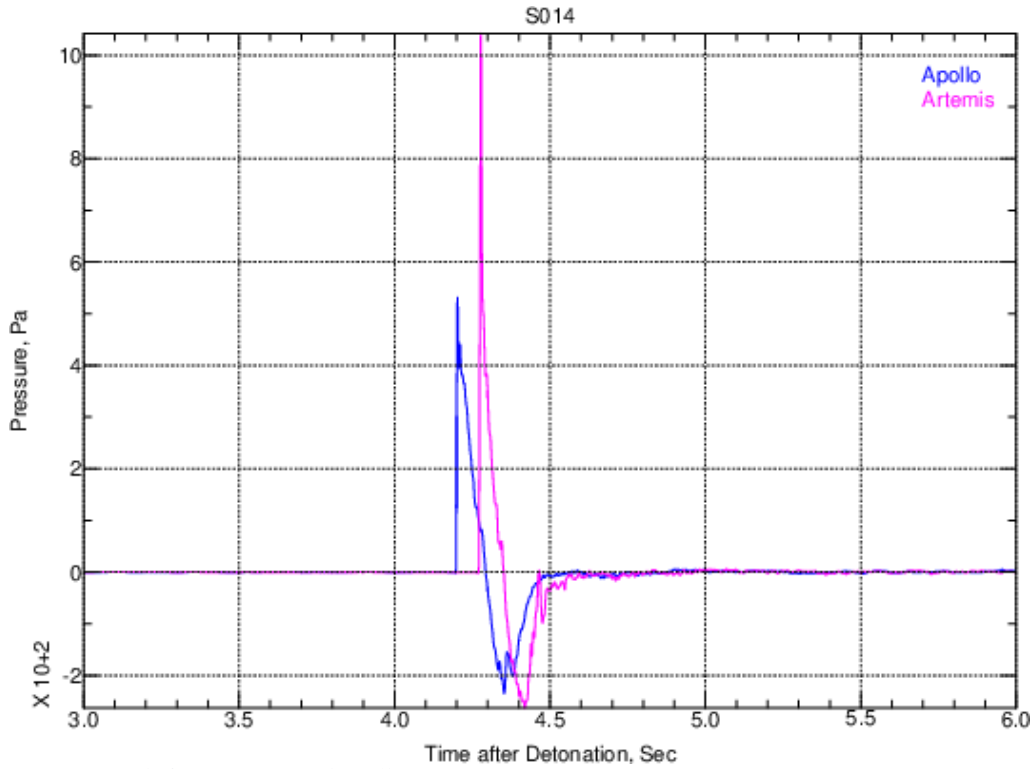

Figure 21. Acoustic signals from Artemis and Apollo at S014.

©2022 Applied Research Associates, Inc. (ARA)

All contents subject to the warning(s) on the title page of this document.

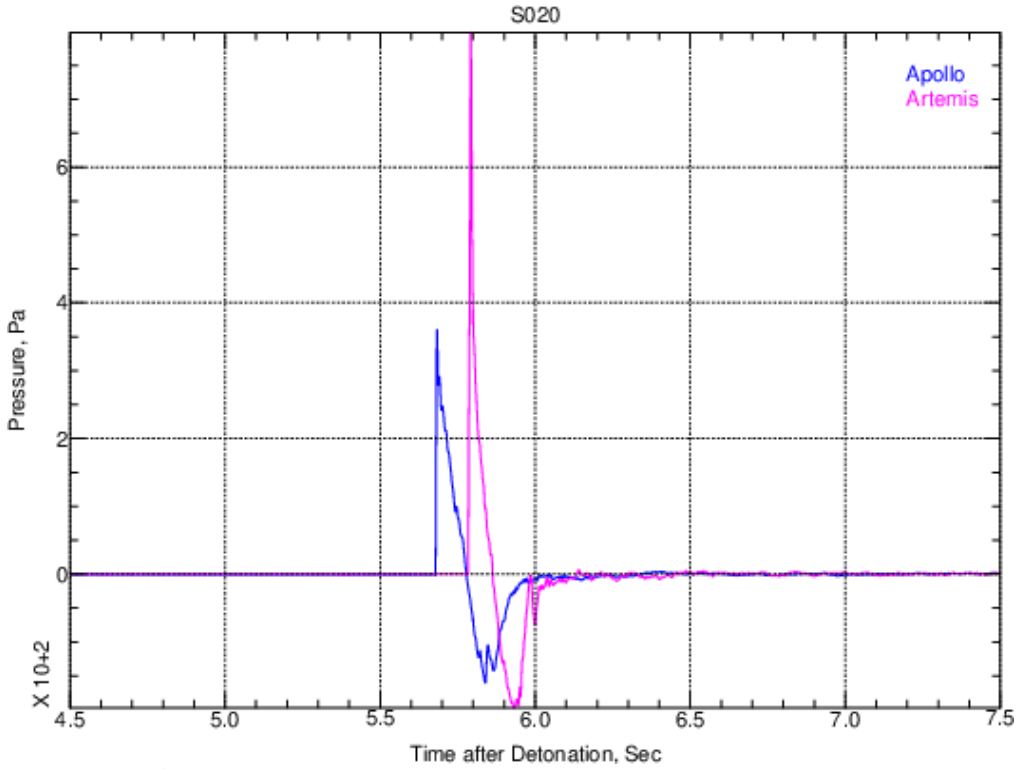

Figure 22. Acoustic signals from Artemis and Apollo at S020.

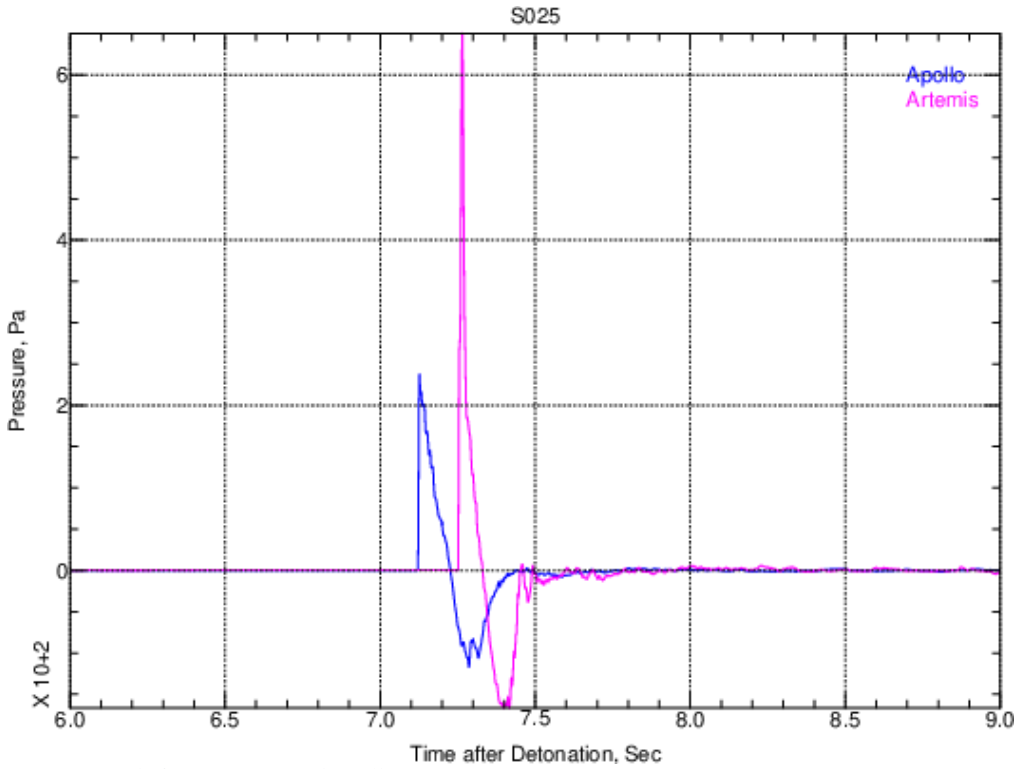

Figure 23. Acoustic signals from Artemis and Apollo at S025.

©2022 Applied Research Associates, Inc. (ARA)

All contents subject to the warning(s) on the title page of this document.

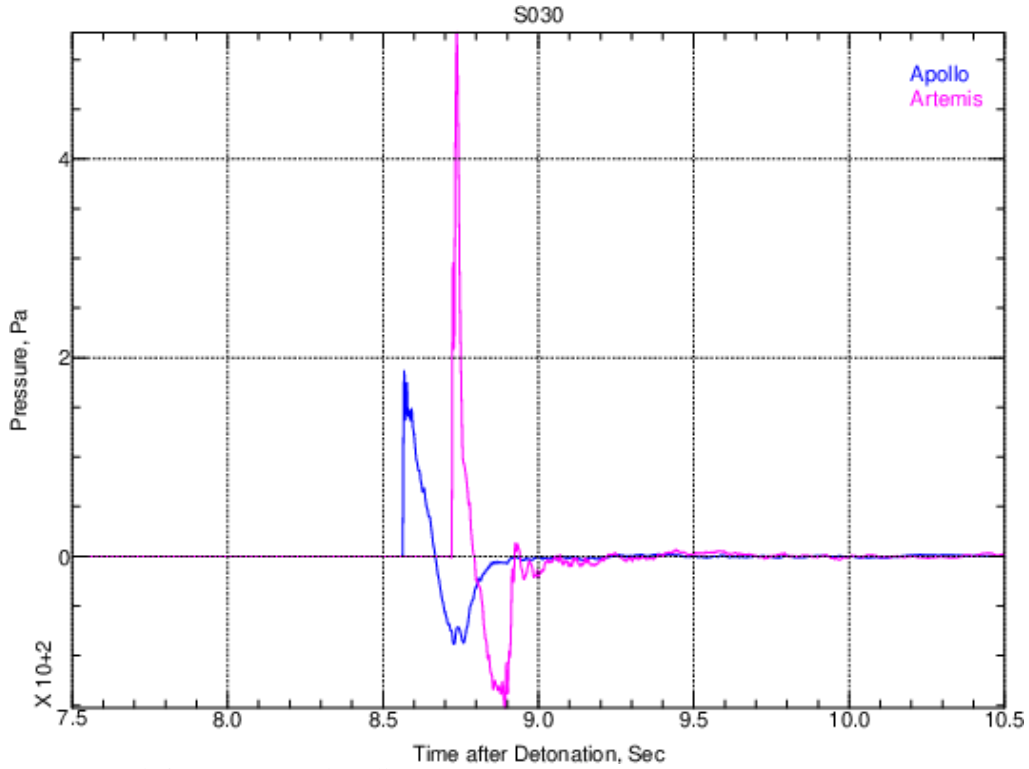

Figure 24. Acoustic signals from Artemis and Apollo at S030.

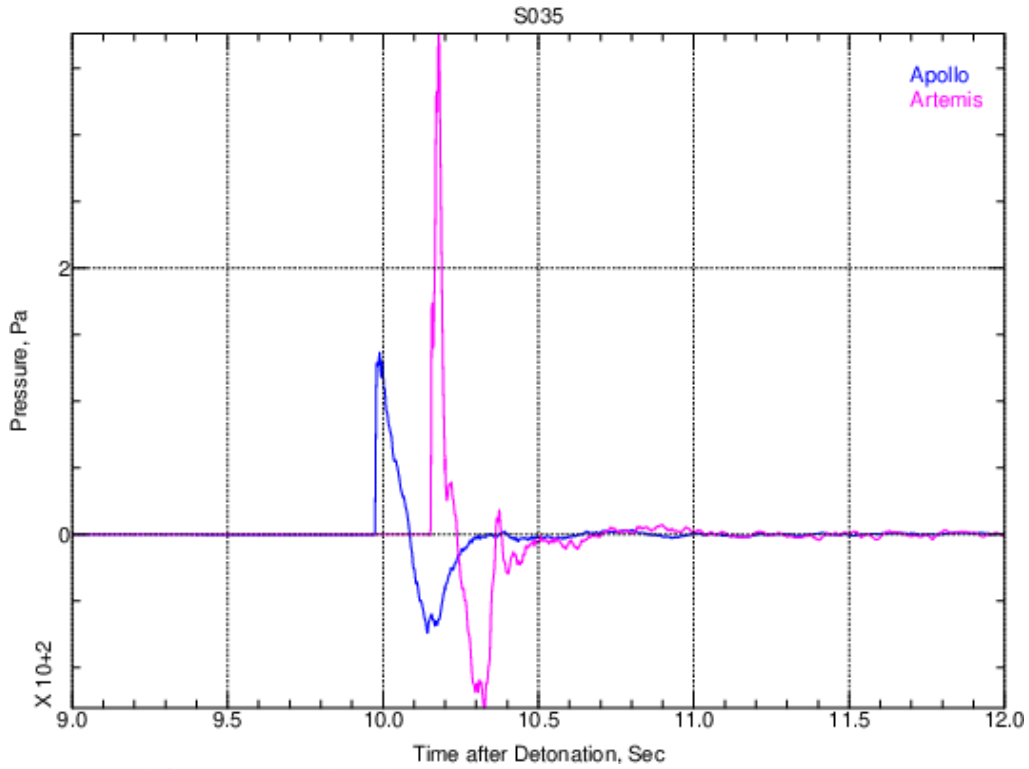

Figure 25. Acoustic signals from Artemis and Apollo at S035.

©2022 Applied Research Associates, Inc. (ARA)

All contents subject to the warning(s) on the title page of this document.

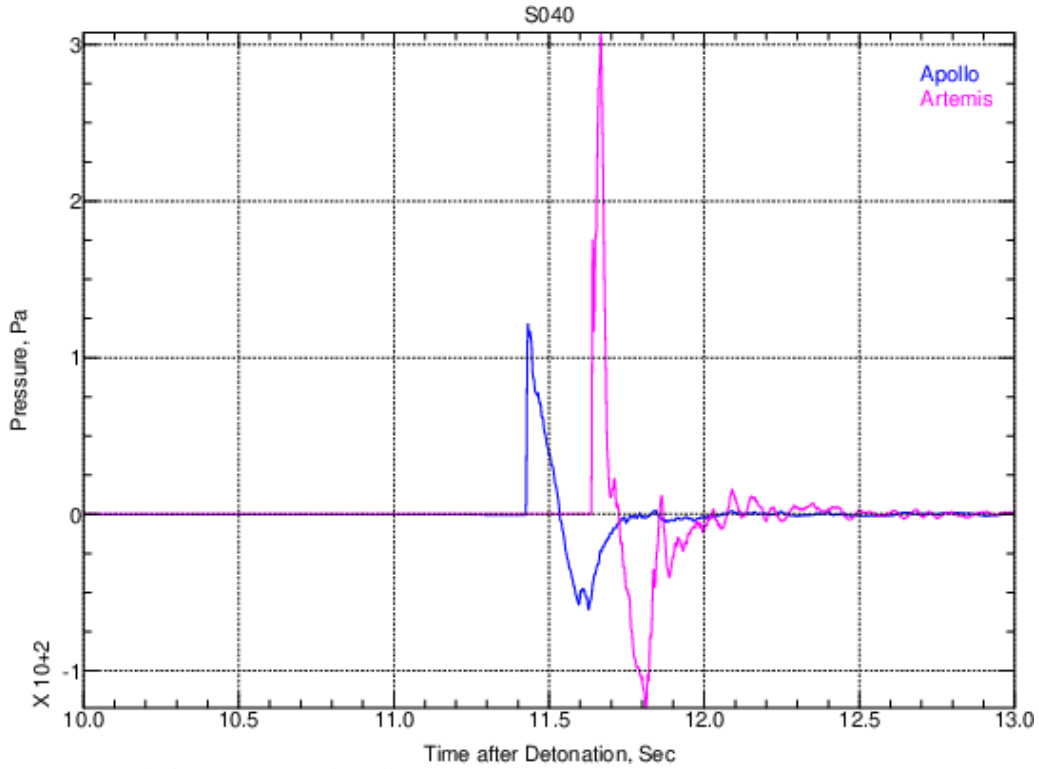

Figure 26. Acoustic signals from Artemis and Apollo at S040.

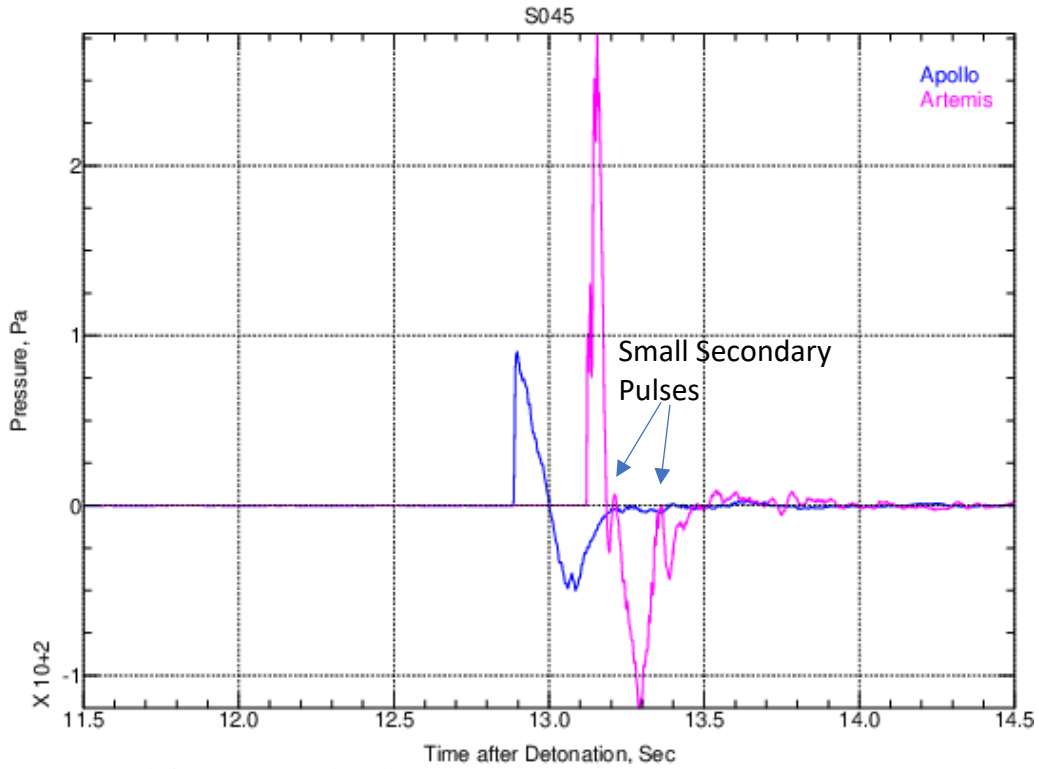

Figure 27. Acoustic signals from Artemis and Apollo at S045.

©2022 Applied Research Associates, Inc. (ARA)

All contents subject to the warning(s) on the title page of this document.

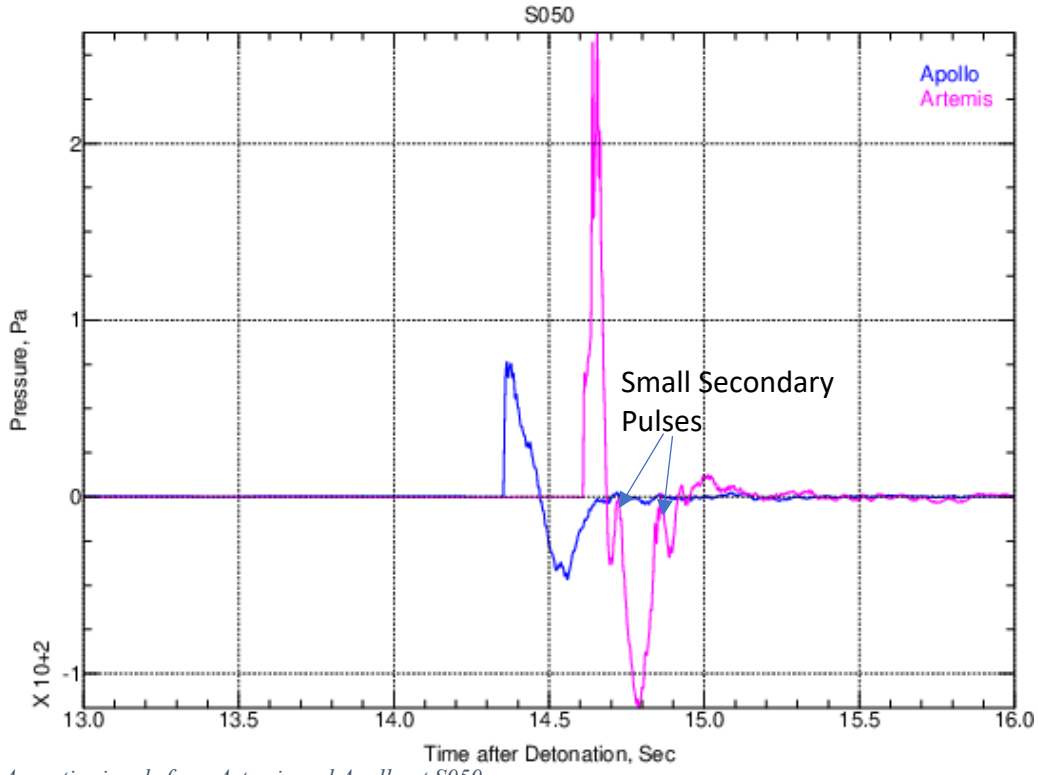

Figure 28. Acoustic signals from Artemis and Apollo at S050.

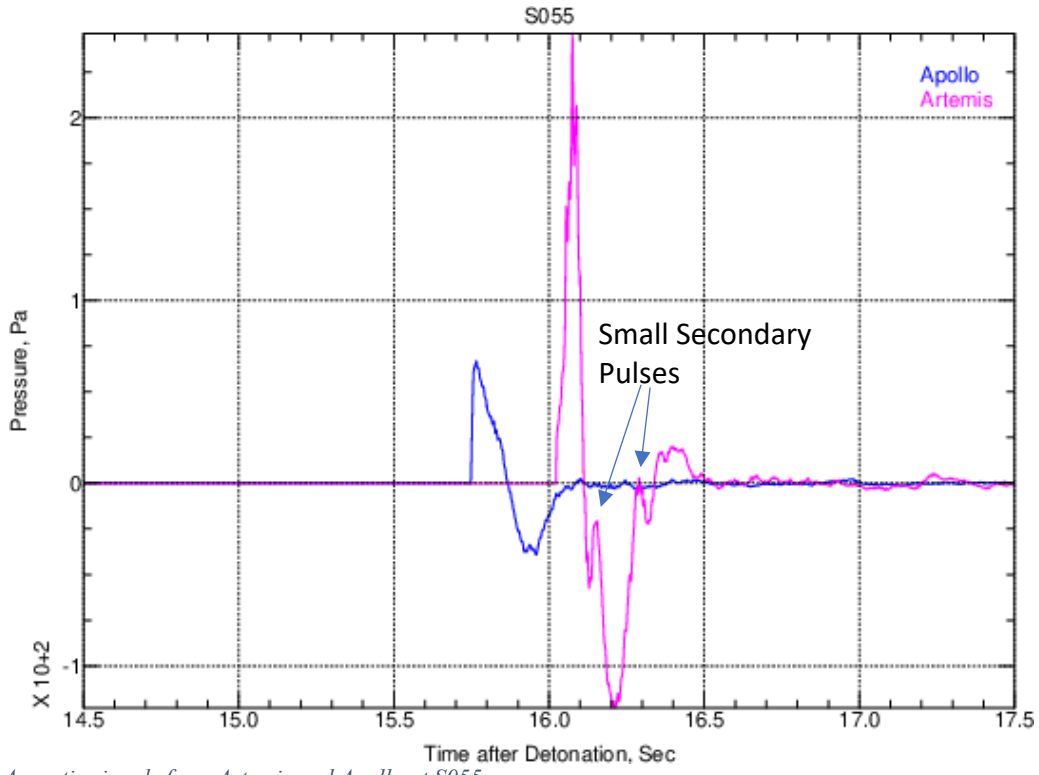

Figure 29. Acoustic signals from Artemis and Apollo at S055.

©2022 Applied Research Associates, Inc. (ARA)

All contents subject to the warning(s) on the title page of this document.

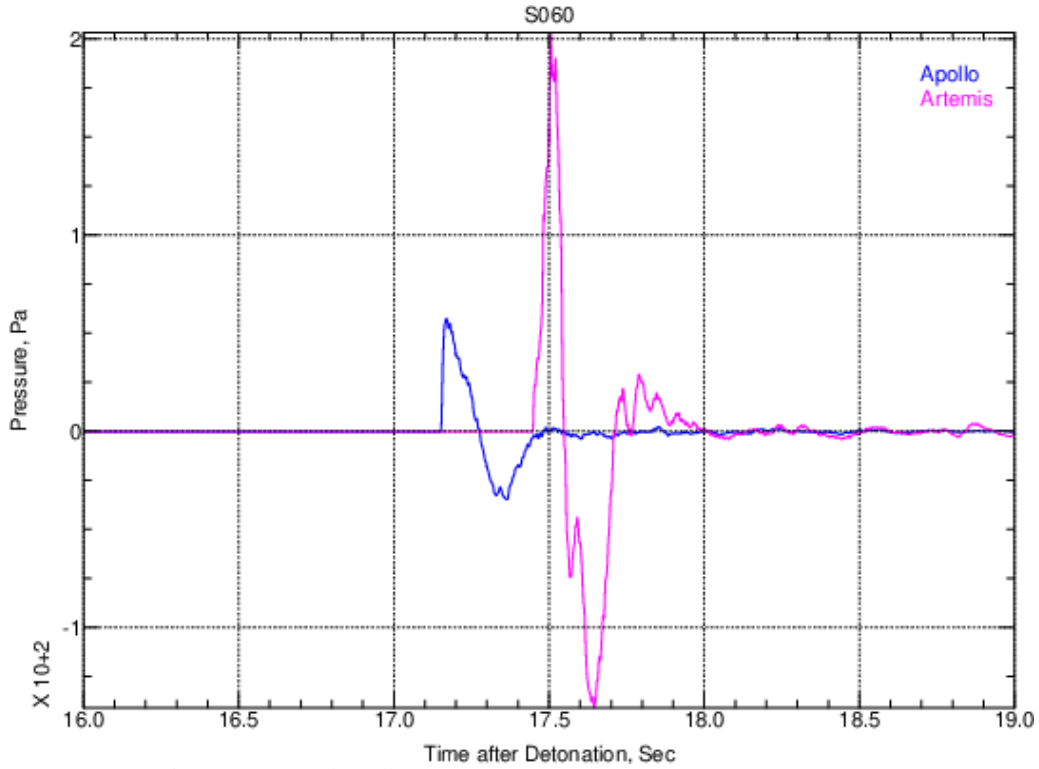

Figure 30. Acoustic signals from Artemis and Apollo at S060.

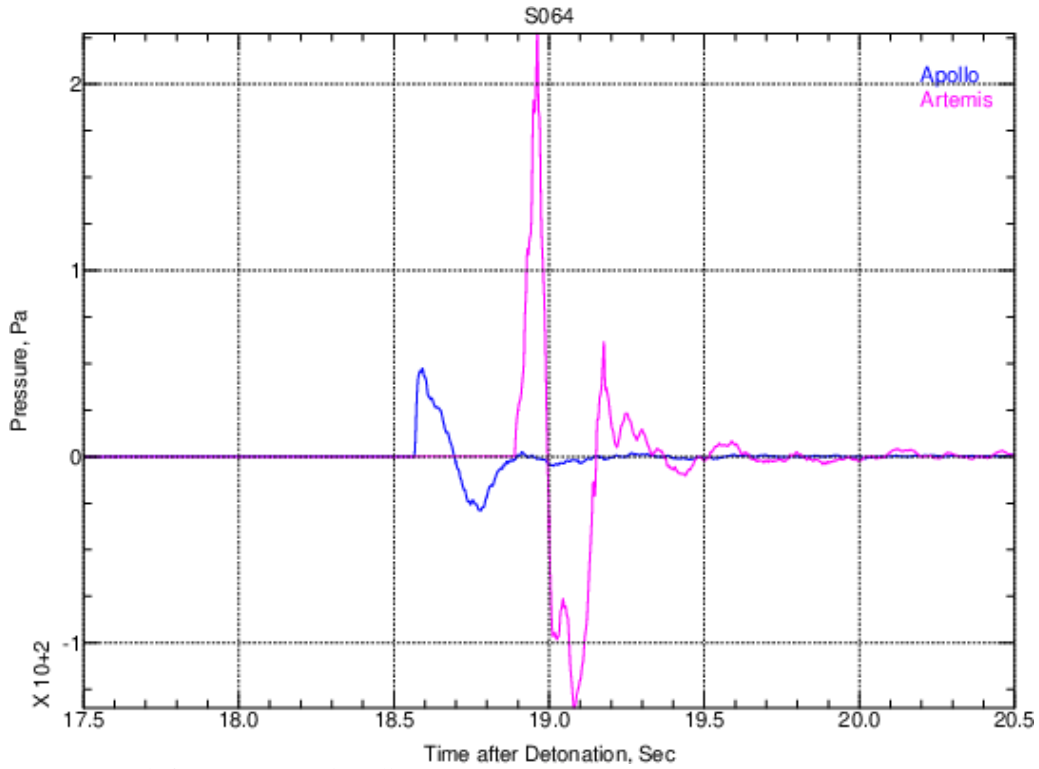

Figure 31. Acoustic signals from Artemis and Apollo at S064.

©2022 Applied Research Associates, Inc. (ARA)

All contents subject to the warning(s) on the title page of this document.

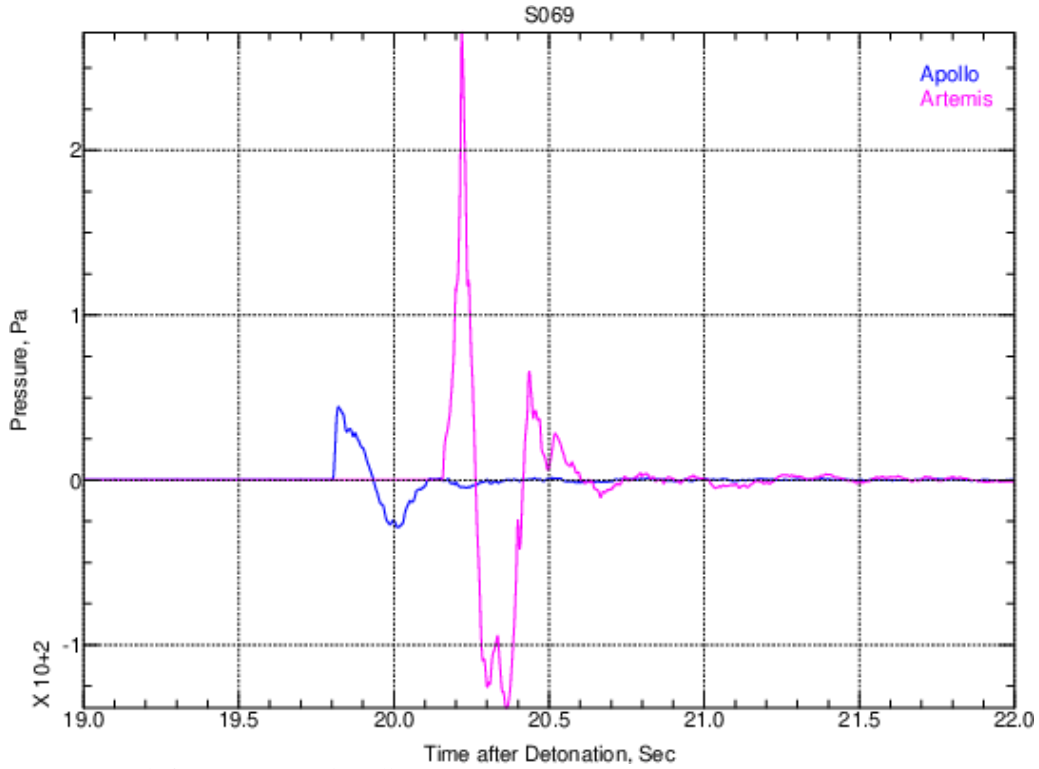

Figure 32. Acoustic signals from Artemis and Apollo at S069.

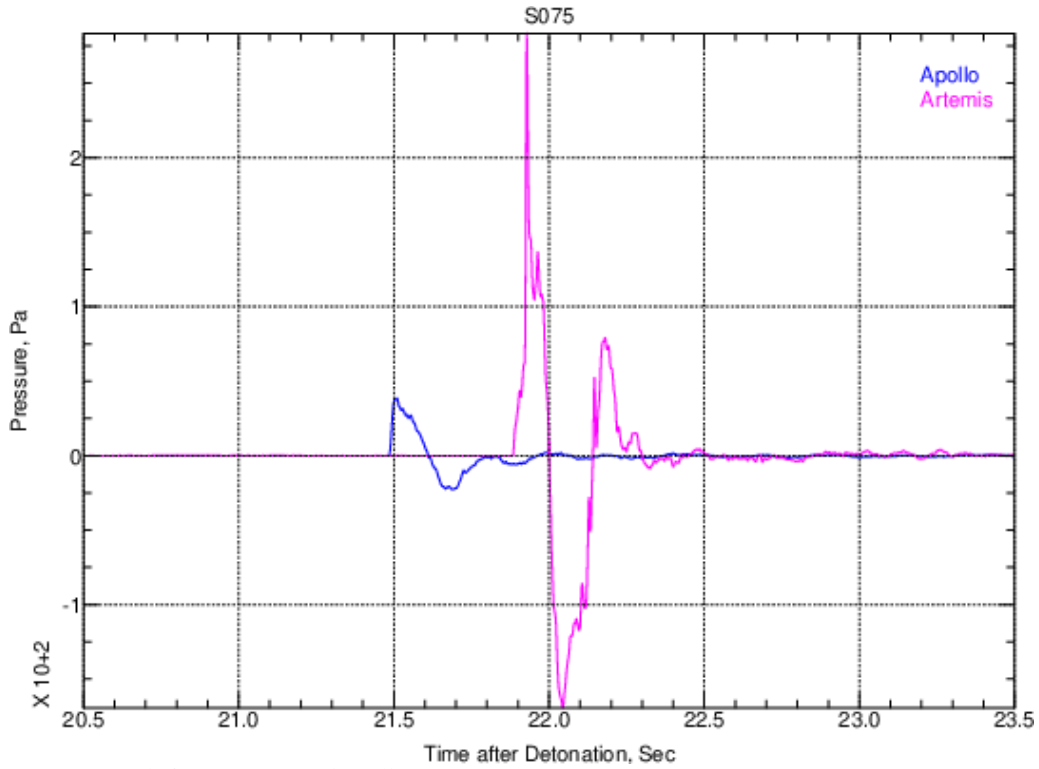

Figure 33. Acoustic signals from Artemis and Apollo at S075.

©2022 Applied Research Associates, Inc. (ARA)

All contents subject to the warning(s) on the title page of this document.

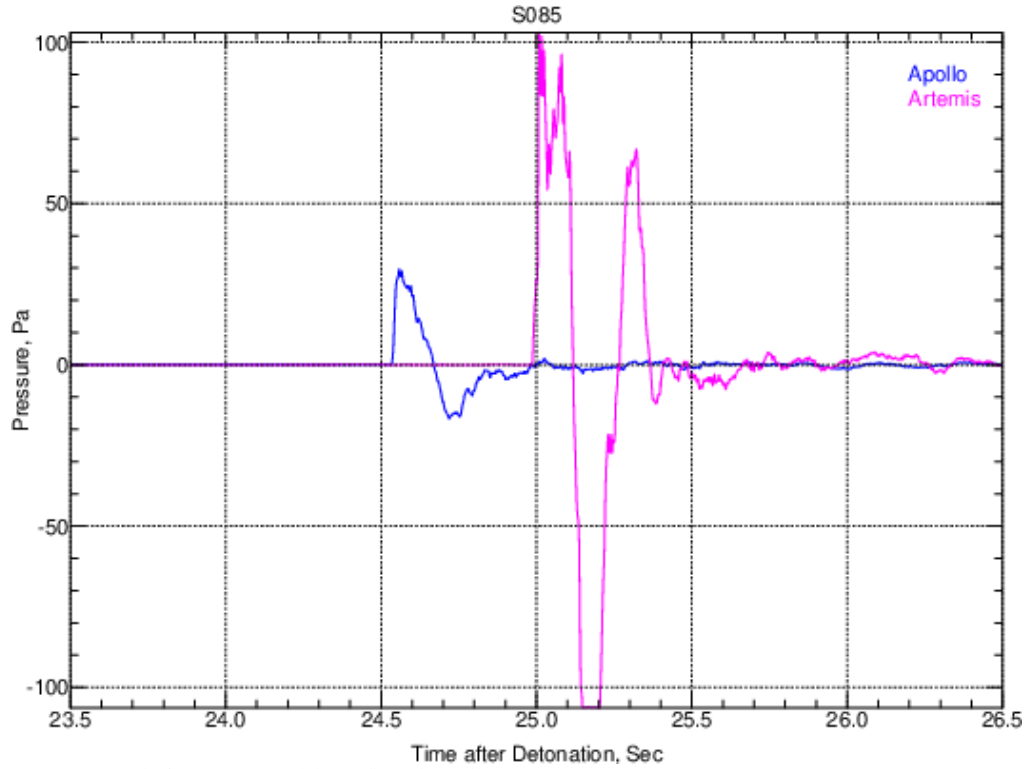

Figure 34. Acoustic signals from Artemis (clipped) and Apollo at S085.

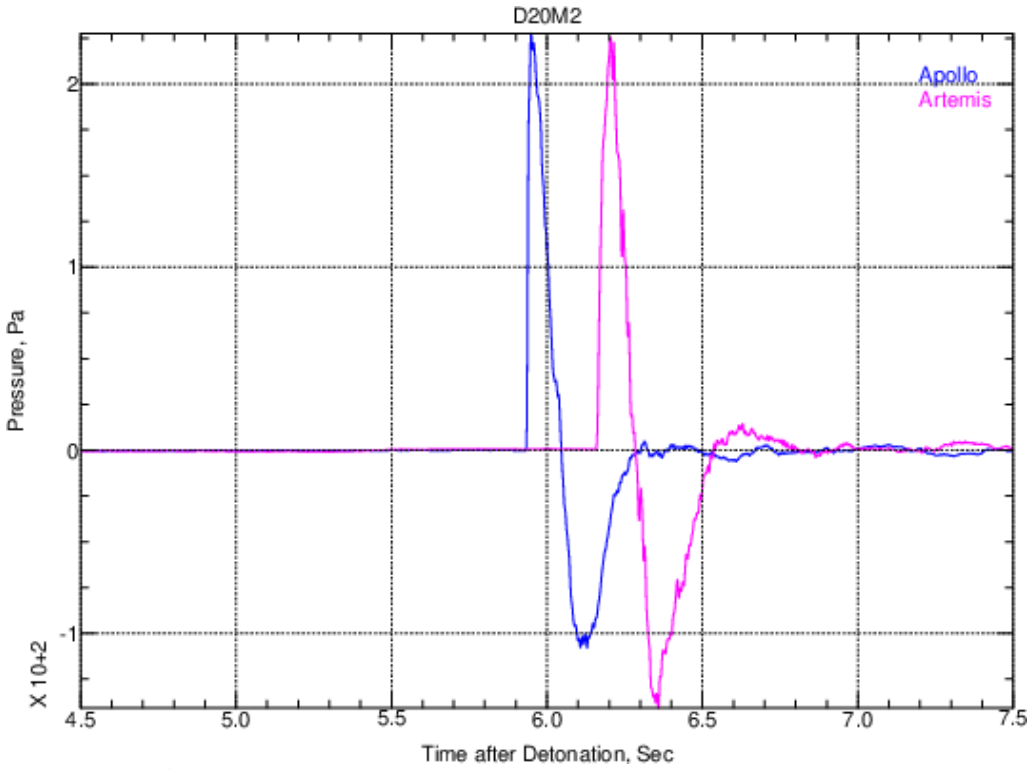

Figure 35. Acoustic signals from Artemis and Apollo at D20M2.

©2022 Applied Research Associates, Inc. (ARA)

All contents subject to the warning(s) on the title page of this document.

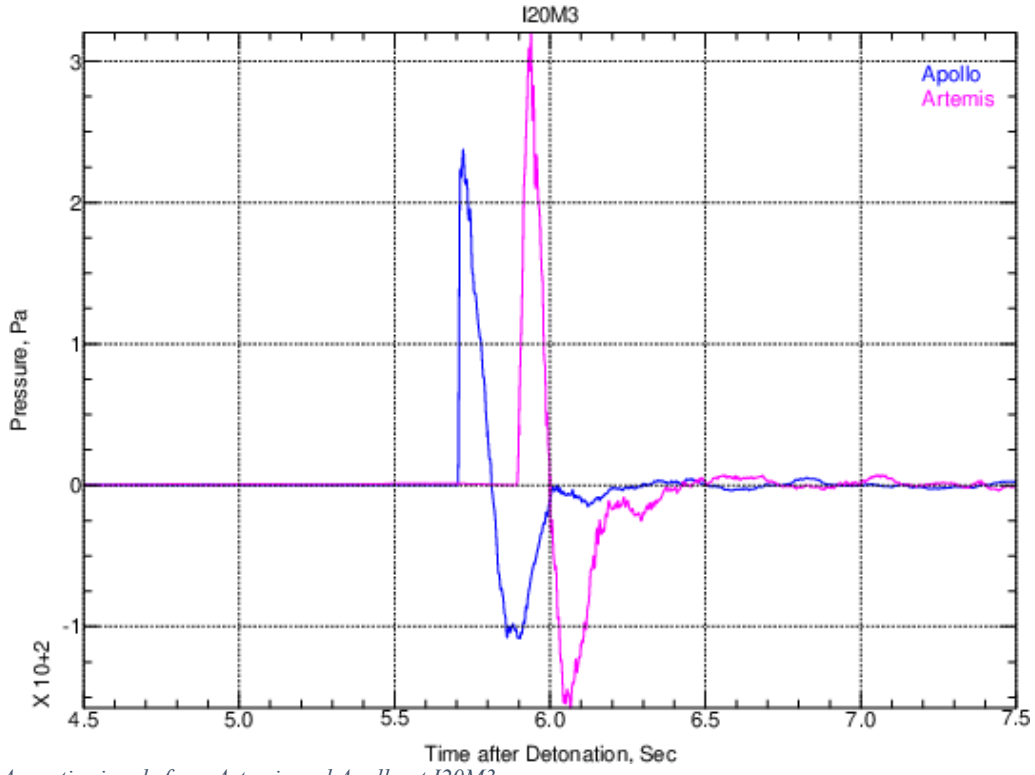

Figure 36. Acoustic signals from Artemis and Apollo at I20M3.

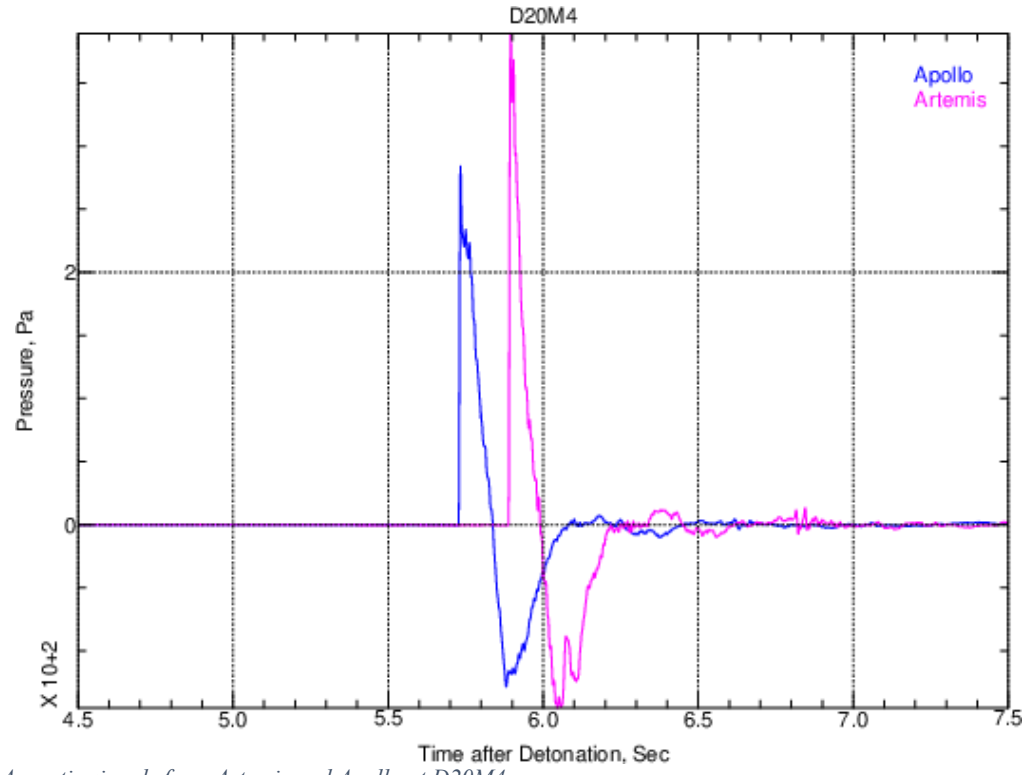

Figure 37. Acoustic signals from Artemis and Apollo at D20M4.

©2022 Applied Research Associates, Inc. (ARA)

All contents subject to the warning(s) on the title page of this document.

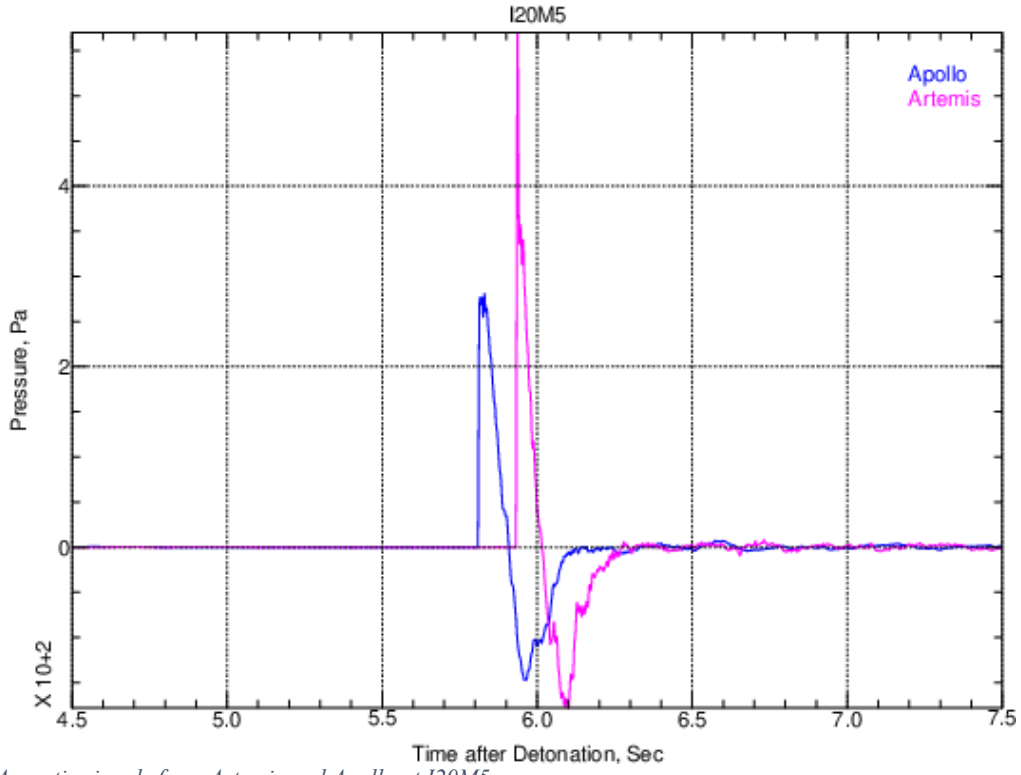

Figure 38. Acoustic signals from Artemis and Apollo at I20M5.

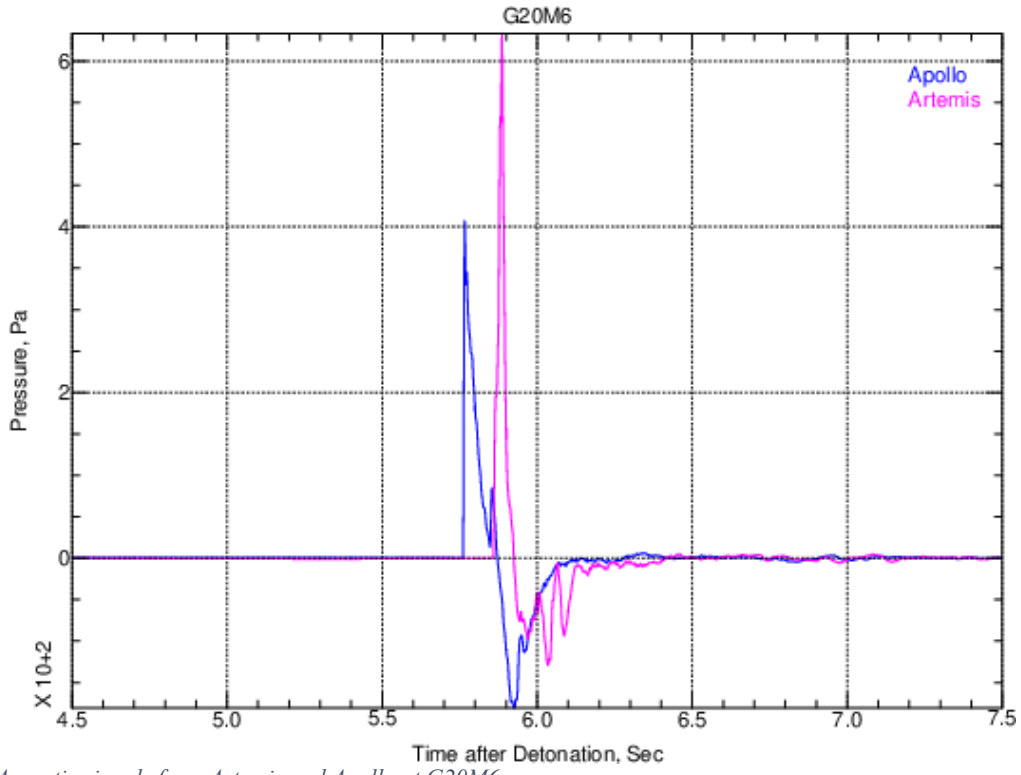

Figure 39. Acoustic signals from Artemis and Apollo at G20M6.

©2022 Applied Research Associates, Inc. (ARA)

All contents subject to the warning(s) on the title page of this document.

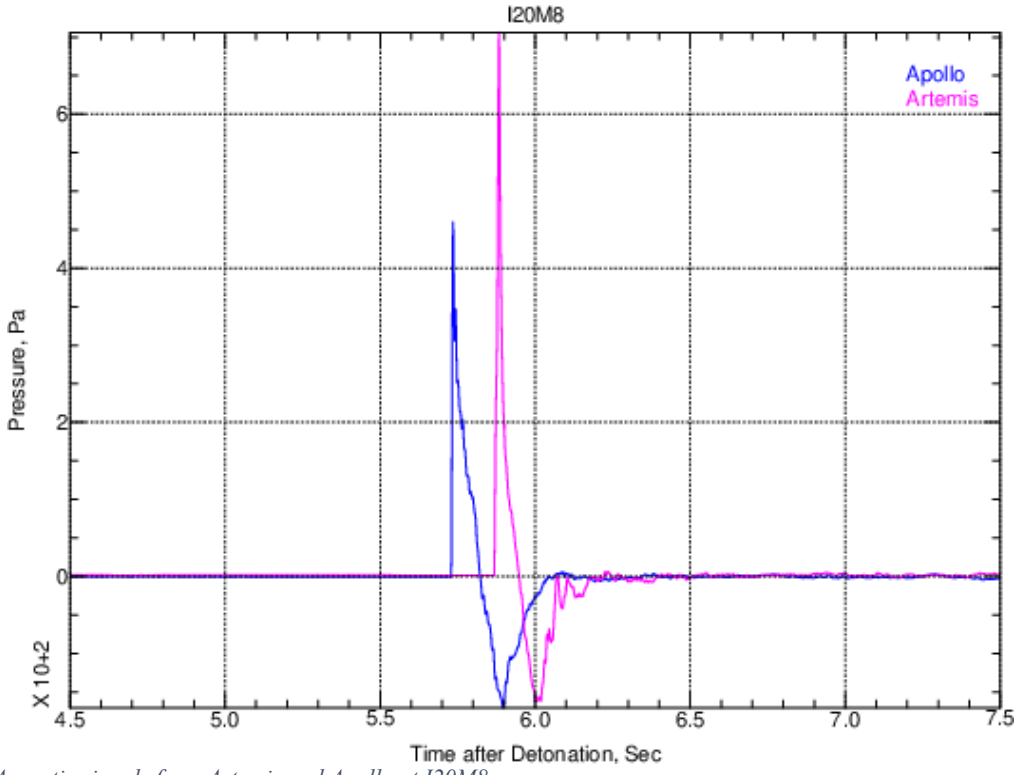

Figure 40. Acoustic signals from Artemis and Apollo at I20M8.

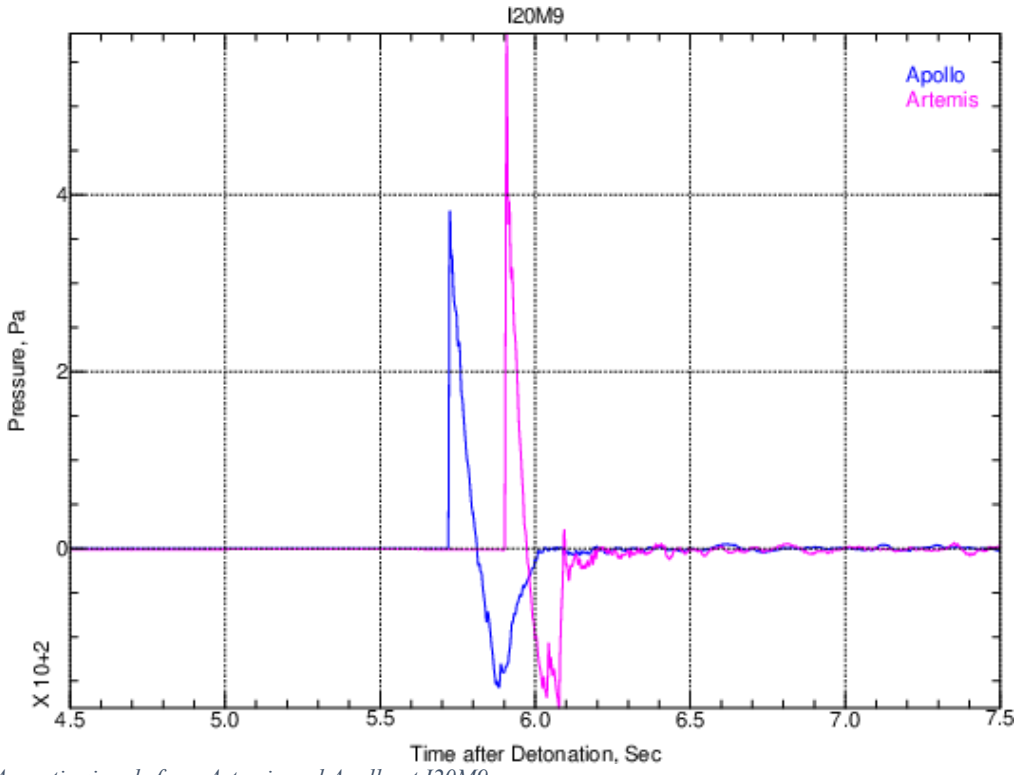

Figure 41. Acoustic signals from Artemis and Apollo at I20M9.

©2022 Applied Research Associates, Inc. (ARA)

All contents subject to the warning(s) on the title page of this document.

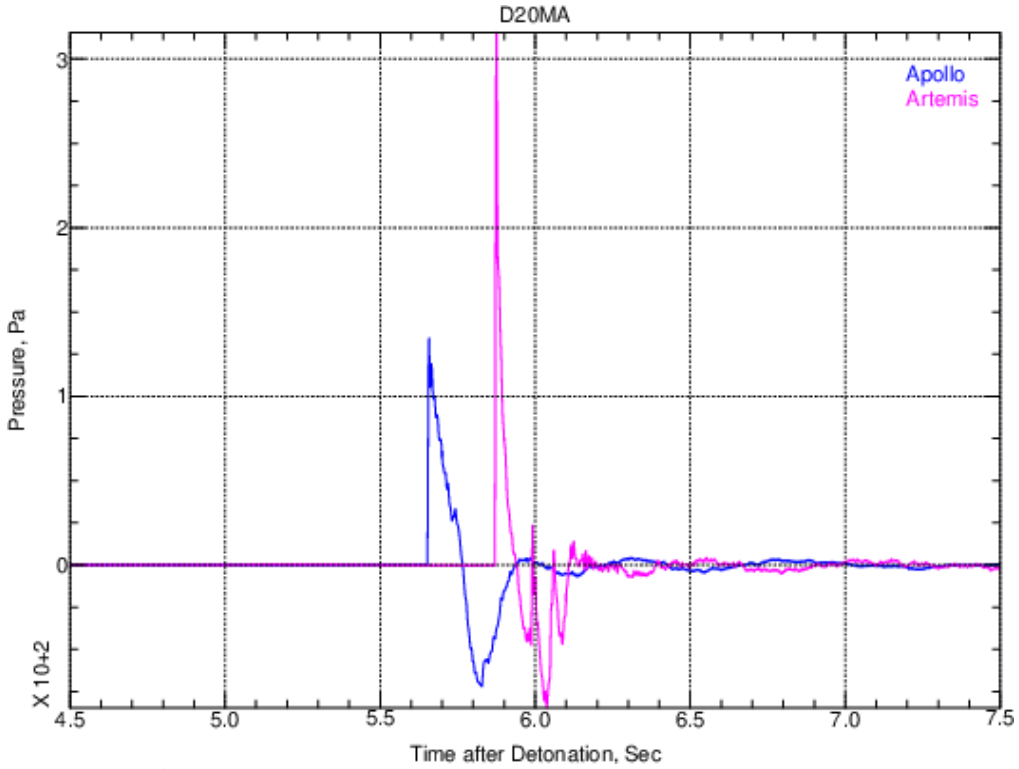

Figure 42. Acoustic signals from Artemis and Apollo at D20MA.

Data Issues

The N035 site successfully recorded the Artemis test, but only recorded digitizer noise for the Apollo test due to a sensor connection issue. The Artemis pressure exceeded the 100 Pa sensor limit at S085 due to the inversion layer and wind blowing towards the sensor from the GZ. Clipping at this site was a known risk during planning, but we decided to continue forward with this sensor at S085, since higher pressure sensors were not available. Scrutiny of the D20MA Apollo recording is warranted based on lower observed pressures relative to nearby sensors.

©2022 Applied Research Associates, Inc. (ARA)

All contents subject to the warning(s) on the title page of this document.

4. Appendix A

Table 5. ARA LSECE Station/Sensor Information.

Station	Lat (WGS84)	Lon (WGS84)	Elev (m)	Digitizer	Bit Weight (V/c)	Sensor	Sensitivity (Pa/V)
N039_WG.	37.14879	-116.08298	1326	RefTek Wrangler	3.720E-08	Hyperion IFS-5311	0.014620
N035_WG.	37.14510	-116.08148	1324	RefTek Wrangler	3.720E-08	Hyperion IFS-5311	0.014510
N029_WG.	37.14011	-116.07944	1314	RefTek Wrangler	3.720E-08	Hyperion IFS-5311	0.014540
N025_WG.	37.13629	-116.07786	1311	RefTek 130S	2.761E-06	Hyperion IFS-5311	0.014690
N020_WG.	37.13238	-116.07652	1299	RefTek 130S	2.761E-06	Hyperion IFS-5311	0.000483
N015_WG.	37.12771	-116.07478	1306	RefTek 130S	2.760E-06	Hyperion IFS-5311	0.000479
N010_WG.	37.12298	-116.07420	1299	RefTek 130S	2.760E-06	Hyperion IFS-5311	0.000483
S009_WG.	37.10631	-116.06633	1275	RefTek 130S	2.757E-06	Hyperion IFS-5311	0.000478
S014_WG.	37.10204	-116.06466	1276	RefTek 130S	2.763E-06	Hyperion IFS-5311	0.000479
S020_WG.	37.09759	-116.06296	1265	RefTek 130S	2.760E-06	Hyperion IFS-5311	0.000478
S025_WG.	37.09327	-116.06126	1267	RefTek 130S	2.760E-06	Hyperion IFS-5311	0.014650
S030_WG.	37.08899	-116.05959	1262	RefTek 130S	2.762E-06	Hyperion IFS-5311	0.014550
S035_WG.	37.08477	-116.05796	1254	RefTek 130S	2.761E-06	Hyperion IFS-5311	0.014600
S040_WG.	37.08047	-116.05612	1249	RefTek 130S	2.758E-06	Hyperion IFS-5311	0.014550
S045_WG.	37.07610	-116.05457	1250	RefTek 130S	2.757E-06	Hyperion IFS-5311	0.014660
S050_WG.	37.07172	-116.05285	1235	RefTek 130	1.582E-06	Hyperion IFS-5311	0.014950
S055_WG.	37.06758	-116.05116	1244	RefTek 130	1.583E-06	Hyperion IFS-5311	0.014580
S060_WG.	37.06336	-116.04958	1233	RefTek 130	1.583E-06	Hyperion IFS-5311	0.014630
S064_WG.	37.05912	-116.04794	1234	RefTek 130	1.583E-06	Hyperion IFS-5311	0.014820
S069_WG.	37.05545	-116.04646	1238	RefTek 130	1.584E-06	Hyperion IFS-5311	0.014770
S075_WG.	37.05042	-116.04446	1232	RefTek 130	1.585E-06	Hyperion IFS-5311	0.014620
S085_WG.	37.04134	-116.04081	1223	RefTek 130S	2.763E-06	Hyperion IFS-5311	0.138580
D20M2_WG.	37.12835	-116.05296	1281	Hyperion	3	Hyperion IFS-5311	0.002791

©2022 Applied Research Associates, Inc. (ARA)

All contents subject to the warning(s) on the title page of this document.

Station	Lat (WGS84)	Lon (WGS84)	Elev (m)	Digitizer	Bit Weight (V/c)	Sensor	Sensitivity (Pa/V)
D20M4_WG.	37.10966	-116.04751	1263	Hyperion	3	Hyperion IFS-5311	0.002953
D20MA_WG.01	37.12144	-116.09006	1307	Hyperion	3	Hyperion IFS-5311	0.000479
D20MA_WG.02	37.12144	-116.09006	1307	Hyperion	3	Hyperion IFS-5311	0.002879
G20M6_WG.	37.09856	-116.07932	1281	Hyperion	3	Hyperion IFS-5311	0.000464
I20M3_WG.	37.11608	-116.04670	1277	Hyperion	3	Hyperion IFS-5311	0.002960
I20M5_WG.	37.10091	-116.05430	1259	Hyperion	3	Hyperion IFS-5311	0.000486
I20M8_WG.01	37.10570	-116.08877	1297	Hyperion	3	Hyperion IFS-5311	0.002879
I20M8_WG.02	37.10570	-116.08877	1297	Hyperion	3	Hyperion IFS-5311	0.000471
I20M9_WG.01	37.11331	-116.09174	1298	Hyperion	3	Hyperion IFS-5311	0.014660
I20M9_WG.02	37.11331	-116.09174	1298	Hyperion	3	Hyperion IFS-5311	0.000479

ARA
©2022 Applied Research Associates, Inc. (ARA)
All contents subject to the warning(s) on the title page of this document.

5. Appendix B

Table 6. ARA Station Operating Period in 2020.

Station	Times of Operation (DOY:HR, UTC)
N039_WG.	300:20 - 314:19
N035_WG.	286:22 - 314:20
N029_WG.	286:22 - 314:20
N025_WG.	286:23 - 314:20
N020_WG.	286:23 - 314:20
N015_WG.	288:19 -314:20
N010_WG.	288:19 - 314:19
S009_WG.	287:23 - 314:18
S014_WG.	287:22 - 314:18
S020_WG.	287:22 - 314:18
S025_WG.	287:22 - 314:17
S030_WG.	287:21 - 314:17
S035_WG.	287:21 - 314:17
S040_WG.	287:20 - 314:17
S045_WG.	287:20 - 314:16
S050_WG.	287:19 - 314:16
S055_WG.	287:19 - 314:16
S060_WG.	287:19 - 314:16
S064_WG.	287:18 - 314:15
S069_WG.	287:18 - 314:15
S075_WG.	287:17 - 314:15
S085_WG.	287:16 - 314:14
D20M2_WG.	289:18 - 314:18
D20M4_WG.	289:17 - 314:17
D20MA_WG.01	288:17 - 300:16
D20MA_WG.02	300:17 - 314:18
G20M6_WG.	289:22 - 314:16
I20M3_WG.	288:17 - 314:17
I20M5_WG.	288:23 - 314:17
I20M8_WG.01	288:17 - 300:16
I20M8_WG.02	300:17 - 314:15
I20M9_WG.01	289:23 - 300:16
I20M9_WG.02	300:17 - 314:15

Attachment 2

Schalk, W., 2020. Written Communication prepared by the NNSS Weather Operations, Air Resources Laboratory/Special Operations and Research Division. LSECE and BEEF Weather Data Collection. Mercury, NV.

LSECE and BEEF Weather Data
10/27/2020, 10/29/2020, 11/07/2020

Walt Schalk, NOAA ARL/SORD
NNSS Weather

ARL/SORD collected the following weather data during the LSECE and BEEF Experiment.

- NNSS Mesonet (MEDA) data from six semi-permanent stations (10-meter towers), Figure 1.
    - Station ID,
    - Date/Time (in PST) stamp (yyyymmddhhmmss),
    - Wind Speed at 10 meters (meters/second, m/s), 15-minute average,
    - Wind Direction at 10 meters (degrees), 15-minute average,
    - Sigma Theta (unitless, the variation of the wind direction), 15-minute average,
    - Minimum Wind Speed in 15-minute period (m/s),
    - Maximum Wind Speed, Gust, in 15-minute time period (m/s),
    - Temperature at 2 meters (degrees Celsius), 15-minute average,
    - Relative Humidity at 2 meters (%), 15-minute average,
    - Temperature at 8.5 meters (degrees Celsius), 15-minute average,
    - Relative Humidity at 8.5 meters (%), 15-minute average,
    - Atmospheric Pressure at 2 meters (millibars or hectoPascals), 15-minute average,
    - Precipitation (inches), 15-minute total,
    - Dewpoint Temperature at 2 meters (degrees Celsius), 15-minute average, and
    - dT/dz, change in temperature vertically (degrees Celsius/meter), 15-minute average,

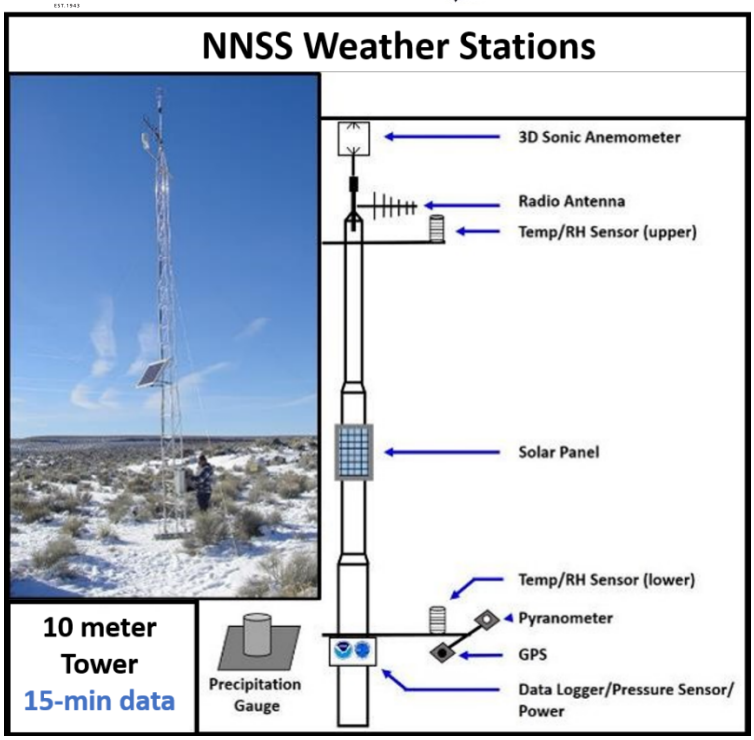

Figure 1. Design of the weather stations on the NNSS.

The data collected are provided in the following files.

- NNSS Mesonet (MEDA) data from six semi-permanent stations (10-meter towers)
  - Filenames:
    - M09_A09AB_10272020.xlsx
    - M09_A09AB_10292020.xlsx
    - M09_A09AB_11072020.xlsx
    - M17_A01AB_10272020.xlsx
    - M17_A01AB_10292020.xlsx
    - M17_A01AB_11072020.xlsx
    - M43_A06AE_10272020.xlsx
    - M43_A06AE_10292020.xlsx
    - M43_A06AE_11072020.xlsx
    - M45_A01AA_10272020.xlsx
    - M45_A01AA_10292020.xlsx
    - M45_A01AA_11072020.xlsx
    - M48_A10AA_10272020.xlsx
    - M48_A10AA_10292020.xlsx
    - M48_A10AA_11072020.xlsx
    - M49_A04AA_10272020.xlsx
    - M49_A04AA_10292020.xlsx
    - M49_A04AA_11072020.xlsx

  - Excel format.
  - Provides a listing of the 15-minute averaged data collected every 15 minutes.
- Lightning Data
  - No Lightning was detected during this experiment.

The location of the NNSS Mesonet (MEDA) stations are as follows in Chart 1 and Figure 1.

Chart 1. NNSS Weather Station (MEDA, M##) information

Station ID1	Station ID2	Station Type	Tower Height (m)	Latitude (degrees N)	Longitude (degrees W)	Elevation (meters)
M09	A09AB	MEDA	10	37.123318	116.042887	1274.0
M17	A01AB	MEDA	10	37.063098	116.053987	1244.9
M43	A06AE	MEDA	10	36.937745	116.037653	1197.3
M45	A01AA	MEDA	10	37.003648	116.059687	1214.6
M48	A10AA	MEDA	10	37.285985	116.044402	1330.8
M49	A04AA	MEDA	10	37.096717	116.088547	1288.1

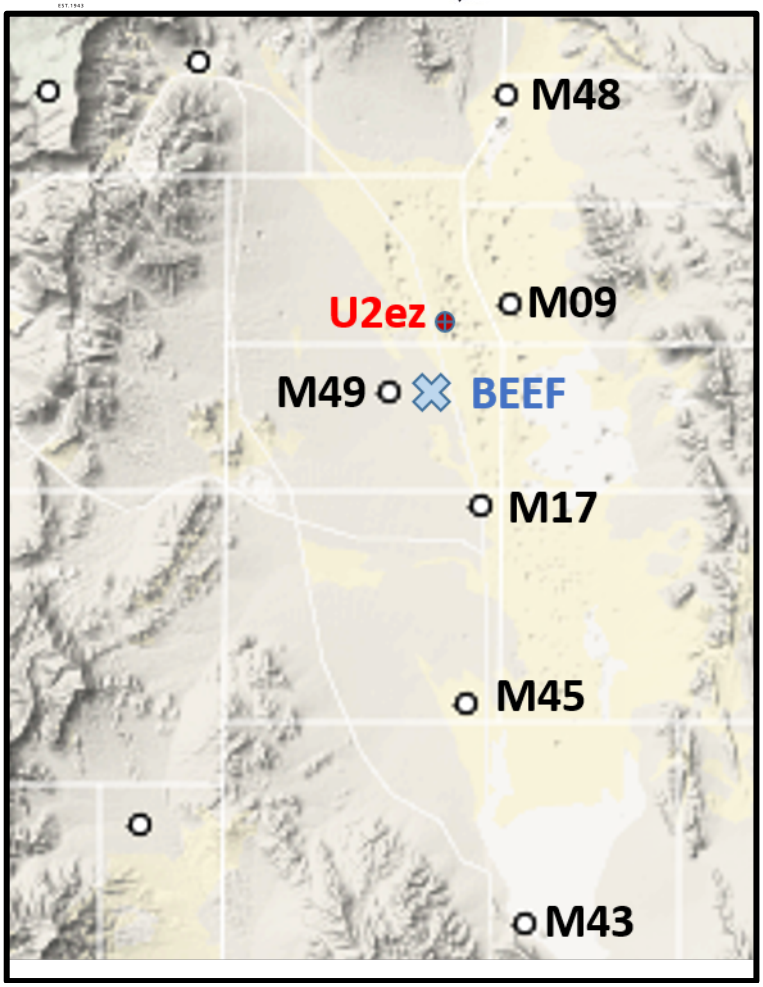

Figure 1. Location of the six NNSS Weather Stations (M##), BEEF, and U2ez.

For questions and comments, please contact:
Walt Schalk
Director, NOAA ARL/SORD
NNSS Weather
702-295-1231
schalk@nv.doe.gov